Characterization of Metal-Insulator-Transition (MIT) Phase Change Materials (PCM) for Reconfigurable Components, Circuits, and Systems

THESIS

Brent L. Danner, Second Lieutenant, USAF

AFIT-ENG-13-M-12

DEPARTMENT OF THE AIR FORCE
AIR UNIVERSITY

AIR FORCE INSTITUTE OF TECHNOLOGY

Wright-Patterson Air Force Base, Ohio

AFIT-ENG-13-M-12

CHARACTERIZATION OF METAL-INSULATOR-TRANSITION (MIT) PHASE CHANGE MATERIALS (PCM) FOR RECONFIGURABLE COMPONENTS, CIRCUITS, AND SYSTEMS

THESIS

Presented to the Faculty

Department of Engineering

Graduate School of Engineering and Management

Air Force Institute of Technology

Air University

Air Education and Training Command

In Partial Fulfillment of the Requirements for the

Degree of Master of Science in Electrical Engineer

Brent L. Danner, BS

Second Lieutenant, USAF

March 2013

AFIT-ENG-13-M-12

CHARACTERIZATION OF METAL-INSULATOR-TRANSITION (MIT) PHASE CHANGE MATERIALS (PCM) FOR RECONFIGURABLE COMPONENTS, CIRCUITS, AND SYSTEMS

Brent L. Danner, BS
Second Lieutenant, USAF

Approved:

Ronald A. Coutu, Jr., Ph.D., P.E. (Chairman) — 4 Mar 13 Date

Derrick Langley, Capt, Ph.D., USAF (Member) — 15 Feb 2013 Date

Alex Li, Ph.D. (Member) — 2/15/2013 Date

Abstract

Many microelectromechanical systems (MEMS) use metal contact micro-switches as part of their reconfigurable device design. These devices utilize a mechanical component that can wear down and fail over time. Metal insulator transition (MIT) materials, also known as phase change materials (PCMs), exhibit a reversible transition that can be used to replace the mechanical component in reconfigurable devices. In the presence of a thermal or electric field stimuli, the PCMs will transition back and forth between a crystalline and amorphous state. During this transformation, the resistivity, reflectivity, and Young's modulus of the material drastically change. This research effort focuses on characterizing the stimuli required to transition germanium telluride (GeTe) and vanadium oxide (VO_x). To do this, test structures were designed and micro-fabricated in AFIT's class 1000 cleanroom. In addition, witness samples were used to characterize the material properties of the PCMs in both their crystalline and amorphous states. The resistivity of the GeTe films underwent a volatile transition from $1.4\times10^{3}\Omega$-cm down to 2.28Ω-cm and a nonvolatile transition from $1.4\times10^{3}\Omega$-cm to $2.43\times10^{-3}\Omega$-cm when a thermal stimulus was applied. The reflectivity of the film also changed significantly when crystallized, increasing over 30%. Lastly, the Young's modulus was measured and showed a 28% change during crystallization. After the materials were characterized, reconfigurable devices were designed to utilize the phase change properties of the PCMs. The results of this research provide a solid foundation for further testing of additional PCMs as well as the ground work necessary for the fabrication of GeTe based reconfigurable circuits, optical components, and MEMS devices.

Acknowledgments

This research effort was only possible with the love and support of my wife. Her endless encouragement helped me through the highs and lows of the last two years. She stood by my side through it all and I could not have done it without her. I would also like to thank my colleagues in the MEMS lab for all the support they provided me. I am also thankful to my advisor, Dr. Coutu, for his help and guidance as well as my committee members who all provided technical insight necessary for my research. I am also extremely grateful to the cleanroom technicians, Mr. Rich Johnston and Mr. Tom Stephenson, for all their help with fabrication and testing.

Brent L. Danner

Table of Contents

Page

List of Figures

Page

List of Tables

Page

Characterization of Metal-Insulator-Transition (MIT) Phase Change Materials (PCM) for Reconfigurable Components, Circuits, and Systems

1. Introduction

Metal insulator transition (MIT) materials are rapidly becoming an important focus in microfabrication and nanotechnology research avenues. Also known as phase change materials (PCMs), these compounds have the ability to be either conductors or insulators depending on various external stimuli applied. This change is induced by an alteration of the atomic structure in the materials as they rapidly transition from an amorphous state to a crystalline state. As this shift in material phase occurs the resistivity of the material changes. Figure 1 (a) is an example of a crystal lattice structure and Figure 1 (b) is an example of an amorphous lattice structure. In the crystal structure, the atoms align, allowing for the material to be less resistive. In the amorphous structure however, the atoms are randomly ordered, making it more difficult for current to travel through the material and therefore making the material more highly resistive. By drastically increasing or decreasing the resistivity of select segments of a wire, a reconfigurable device can be created.

In their amorphous state, some MIT materials have resistivity values of $10^{2}\Omega$-cm. For micro size devices, the resistance values will be in the order of Mega Ohms. With values this high, a wire segment will effectively act as an open circuit or switch. While in a crystalline state, the resistivity of some MIT materials is as low as $10^{-4}\Omega$-cm. These values are not low enough to act as an ideal micro-switch with near zero contact

resistance, but there are many reconfigurable applications that can take advantage of this drastic change in resistivity.

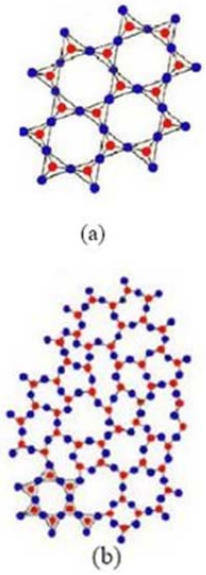

Figure 1: (a) Crystalline lattice structure (b) amorphous lattice structure [1].

In addition to the change in resistivity during the phase transition, optical and structural properties of the PCMs also change. The shift in the atomic structure causes the reflectivity of the materials to change as well as the materials Young's Modulus. By taking advantage of these changes, not only can reconfigurable circuits be created, but also reconfigurable optical devices and reconfigurable mechanical structures.

A variety of materials have been tested and used in a diverse range of applications [2, 3]. PCMs have different transition capabilities and require different types of stimuli in order to achieve these transitions. The Chalcogenide class of PCMs, those that include a group sixteen element, are widely studied for their phase change properties include Germanium Telluride (GeTe) and Germanium Antimony Telluride (GeSbTe). These

compounds are most commonly used in phase change memory applications and require thermal stimuli in order to transition between states. When transitioned, a non-volatile phase change occurs, making them ideal for holding memory states. A variety of Vanadium Oxide (VO_x) phases also exhibit useful phase change properties. Each phase of Vanadium Oxide transitions with the application of different external stimuli, including thermal gradients and electric fields. Vanadium Dioxide (VO_2) and Vanadium Pentoxide (V_2O_5) are the most common phases used as MIT materials. This is because they require the least amount of stimuli in order to transition. The rapid phase transitions that occur in both classes of PCMs make them ideal for use as a reconfigurable component.

1.1 Traditional Reconfigurable Device Issues

Many microelectromechanical systems (MEMS) use metal contact micro-switches as part of their reconfigurable device design. Both DC and RF MEMS devices employ reconfigurable components. These devices often involve a mechanical component, or switch, that can wear down over time. As these switches are actuated, the consistent pounding of the electric contacts generates contamination [4]. These impact forces generated between the top and bottom electrodes also cause damage and hardening of the contacts [5]. Not only will this contamination and damage increase the resistance when the switch is closed, but it also leads to the micro-switches becoming stuck down and no longer able to actuate.

Many micro-switches are actuated using the electrostatic force generated between two biased electrodes. These electrodes are another avenue of potential failure for the

mechanically driven micro-switch, and therefore failure of the reconfigurable component. MEMS switch reliability continues to be a big issue when employed in commercial and government applications [6].

These micro-switches can be used to switch between loads when designing tunable and reconfigurable devices. In these circuits, MEMS components are used to vary the length of wire segments or alter current flow in order to adjust the characteristics of the circuit. While this has proven to be an effective method for tuning devices, the mechanical switching components still have a limited reliability due to contact contamination, material transfer, and stiction [4, 7]. Figure 2 shows an example of material transfer in a gold-gold micro-switch. In order to increase the lifetime of these circuits that utilize micro-switches, the mechanical switching component within the device needs to be removed.

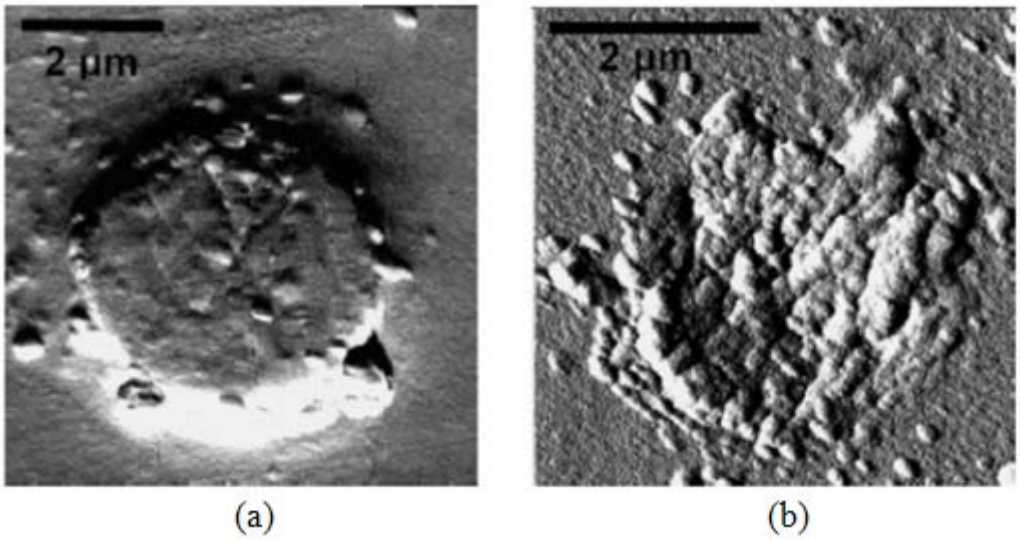

Figure 2: SEM images of damaged gold on gold contact surfaces (a) is top electrode (b) is bottom electrode [7].

1.2 MIT Material Use as a Reconfigurable Component

The ability to transition from an insulator to a conductor can also be used to control the current flow within a circuit. By replacing a traditional mechanical micro-switching component with an MIT wire segment, the circuit can maintain similar operational capabilities. These segments can be designed in a way that the external stimulus required to transition the material can be applied without altering other attributes of the circuit.

Once the MIT wire segment is fabricated within the circuit, the stimulus can be externally applied, altering the state of the reconfigurable device. For designs requiring a true on/off switching mechanism, a MIT material with a large variation between its high and low resistive states is necessary. Since MIT materials do not have the ideal conductivity of a contact material such as gold, the minimal resistance achievable in this new switching component will be slightly elevated. This, however, can be combated by controlling the geometries of the PCM component. In devices that require the ability to tune, or reconfigure, a particular component, it isn't as crucial to get near zero resistance when in the "on" position. The geometry of the MIT wire segment will also play a significant role in the tunable range of the component as well, and therefore must be taken into account when designing the reconfigurable device.

Since micro-switching devices and reconfigurable devices require different attributes from the PCM component, it is extremely important that the materials are characterized in order to create an appropriate device. The material properties in both amorphous and crystalline states need to be known in order to select the best material for the specific design. This will also show the range in which the specific materials can be

transitioned. The type of external stimulus that is required to transition each material is also crucial to the component design. While some materials may transition best with a thermal stimulus, others may show a larger transition when an electric field is applied to the PCM segment. It is also important that the amount of stimulus necessary to achieve the desired transition is known. Specific applications may be sensitive to a flux in temperature within the device, and therefore a MIT material that requires a large thermal stimulus to transition may not be appropriate. Once the stimulus strength necessary to generate a phase transition is known for each of the MIT materials, one can be selected to meet particular design requirements. It is also critical to characterize the affects of the MIT geometries on the transition of the wire segment. Once the required MIT material is selected, it can be fabricated into the device as a wire segment, replacing the traditional micro-switch or reconfigurable component.

While the change in resistivity will be constant for a given MIT material and a specific stimulus, its affect will differ depending if the device is being used in a DC or RF application. For DC applications, as the resistivity of the material increases or decreases, so too will the resistance of the wire segment. This will have a linear impact on the DC current that travels through the wire. In RF applications, the wire segments will initially be impedance matched to the device. By increasing the resistivity of the material, the device will no longer be impedance matched. This will cause more of the power applied to the circuit to be reflected back, while the power through the device will decrease. On the other hand, when the resistivity decreases as the materials transition to their crystalline state, the reflected power will decrease and the power through the device will increase.

In both tunable and on/off designs, the stimulus is altering the atomic structure of the material, not physically moving any parts. Therefore, by removing the mechanical micro-switch failure modes described in [7], the potential for component failure is drastically decreased.

1.3 Methodology and Characterization

In order to fully characterize PCMs and the stimuli required to transition them, micromachined test structures will be designed and fabricated. These devices will be created in a way that allows the resistance of the material to be measured while a thermal and/or electric field stimulus is applied to the MIT wire segments. The test structures designed will be used to characterize different MIT materials, depending on which they are fabricated with. Each type of material will be tested using identical structures, allowing for a direct comparison of the phase transition in the different materials. The RF test structures will utilize a coplanar waveguide (CPW) to measure the signal response during the phase transition. The data collected from these test structures will be tabulated and summarized into a thorough characterization of the MIT materials.

1.4 Summary

MIT materials have a great potential to be used as components suitable for reconfigurable, adaptable and tunable circuits for military and commercial DC and RF systems. The characterization of the stimuli required to transition these materials is necessary prior to them being utilized in real world applications. Once these materials are fully characterized, they can be used to increase the lifetime and reliability of devices that use reconfigurable components by removing the need for mechanical parts.

The following section of this document will detail the background of MIT materials. It will describe previous applications of PCMs as well as some initial testing done by other researchers. Later sections will describe the methodology used for the design of and testing of the novel micro-structures. The resulting data obtained from these structures will then be presented and analyzed. The final section of this document will present conclusions from the experiments performed as well as provide suggestions for future work.

2. Literature Review

2.1 Chapter Overview

In this chapter, the current research of phase change materials (PCMs) will be discussed. The fabrication and testing methods of different PCM applications used by current researchers are explored. While many materials are being used for their metal insulator transitions, this research focuses on the work being done with Germanium Telluride (GeTe) and Vanadium Oxides (VO_x). In addition, reconfigurable applications that can utilize the phase transition of these PCMs are presented.

2.2 Reconfigurable Devices

Reconfigurable devices are extremely useful in designing and fabricating electrical circuits, resonators, optical devices, and numerous other components. The ability to use a single device for multiple applications or to generate multiple responses is very valuable. Not only does it minimize the system cost by removing the need for additional separate devices, but it also allows components to be made even smaller. These devices can be reconfigured using micro-switches, PCMs, or by altering the geometries of the component. By using PCMs, there is no need for a mechanical component, thus increasing the lifetime of the device.

2.2.1 Reconfigurable Circuits

Simple RC filters can be designed by placing a resistor and a capacitor in series. Figure 3 shows a schematic of a RC low-pass filter. By switching the location of the resistor and the capacitor, a high-pass filter can be created.

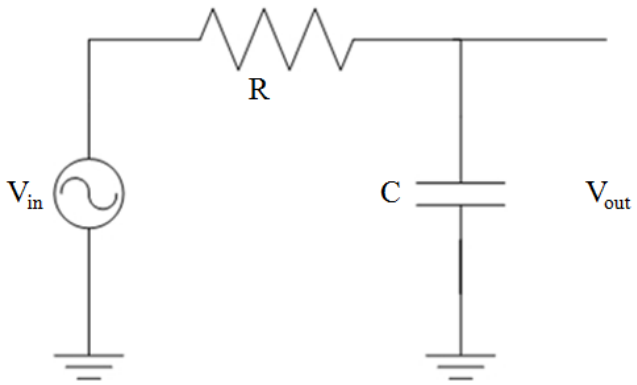

Figure 3: RC low-pass RF filter schematic.

The cut-off frequency of the filter is determined by the resistance and capacitance internal to the circuit. Using Equation 1, the cut-off frequency of both a low pass and high pass filter, depending on the configuration of the circuit, can be calculated [8].

$$f_{cut-off} = \frac{1}{2\pi RC} \quad (1)$$

By changing the resistance or capacitance within the circuit, a tunable filter can be created. When using PCMs as the reconfigurable component, the resistivity and permittivity of the material can be tuned in order to change the cut-off frequency of the filter. As can be seen in Equation 2, the resistance of the filter is directly related to the resistivity, ρ, of the PCM, while the capacitance of the filter is directly related to the relative permittivity of the material, ε_r, as shown in Equation 3. By tuning these material properties of the filter, the cut-off frequency can be tuned without using a mechanical component or altering the geometries of the device.

$$R = \frac{\rho L}{A} \quad (2)$$

$$C = \frac{\varepsilon_r \varepsilon_o A}{d} \quad (3)$$

Reconfigurable RF filters have also been fabricated using MEMS technology and can be used in a variety of compact microwave circuits [9, 10]. Lee *et al.* have demonstrated that using MEMS switches, reconfigurable low-pass filters can be designed and fabricated [11]. Groups of micro-switches are actuated using electrostatic force and depending on which bank of switches is in an "on" state, the capacitance across the device will vary. By using electroplated gold contacts, with a contact resistance of 1.4Ω, and fabricating the structure on a quartz substrate, the insertion loss through the device was minimal. In its initial state, the cut-off frequency of the low-pass filter was 67GHz, as shown in Figure 4 (a). With the MEMS switches actuated, the reconfigured device had a new cut-off frequency of 28GHz, as shown in Figure 4 (b).

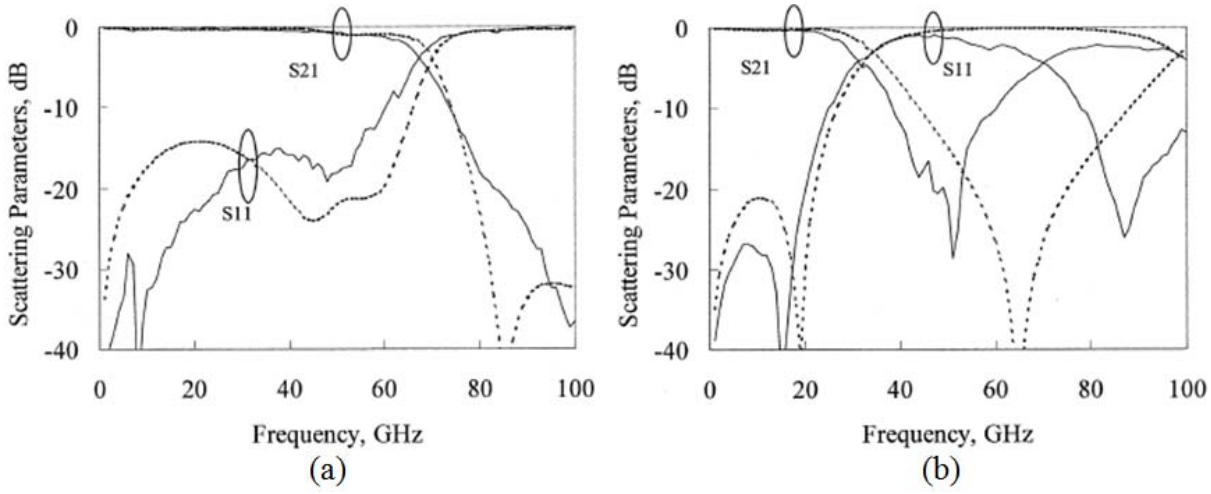

Figure 4: Measured and simulated frequency response of (a) original state and (b) reconfigured state of the low-pass filter. Solid lines are measured results and dotted lines and simulated results [11].

The reconfigurable RC and MEMS based filters described above can also be implemented by using PCMs in lieu of the resistors or mechanical micro-switches. In the

RC circuit design, the PCM material can be used in place of the resistor and when the external stimuli are applied to transition the material, the filter will have a different cut-off frequency. By manipulating the geometries of the PCM component as well as its chemical composition, the resistance values can be tuned to provide a wide-band filter with a reconfigurable range of up to six-orders of magnitude.

The MEMS based filter can be implemented by replacing the micro-switches with PCM components. By using a PCM with a high "off" resistance and large difference in its low and high resistive states, a micro-switching component will be created that can be used to reconfigure the cut-off frequency of the filter. By applying the stimulus required to transition the material, specific PCM components can be "switched" independently. This allows for the different banks of switches to be transitioned in unison in order to reconfigure the filter.

2.2.2 Reconfigurable Optical Devices

Similar to reconfigurable circuits, optical devices can be reconfigured by altering the material properties of a particular component. The type of material used as well as its lattice configuration will impact the amount of light that is reflected off its surface. A photodetector can be used to measure the quantity of light that is given off the sample surface. The detector will then translate the light into an electrical signal. By altering the amount of light that is reflected off the material, the electrical signal can be varied, thus creating a reconfigurable device. A configuration similar to Figure 5 can be used to monitor the reflectivity of a sample or optical device.

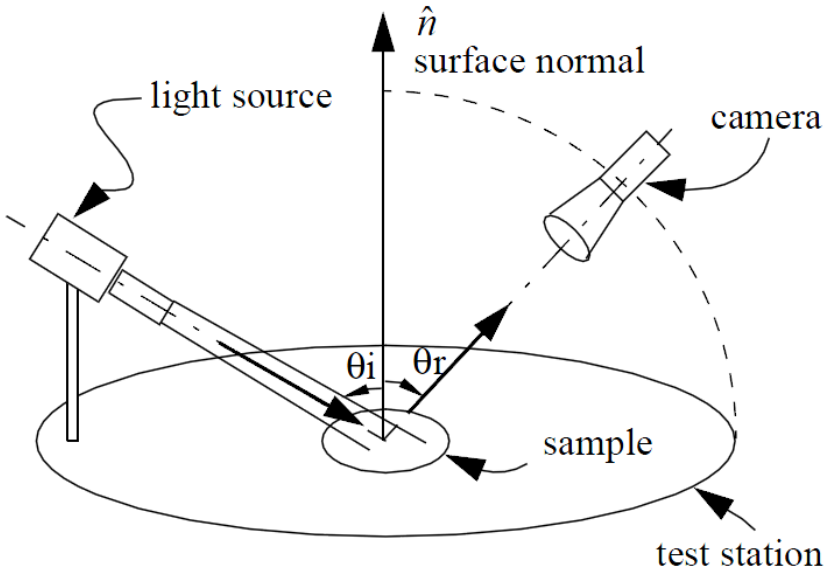

Figure 5: Optical test structure used to monitor the reflectivity of a reconfigurable device [12].

The reflectance of a material, R, can be defined as the ratio of reflected power to the incident power [13].

$$R = \frac{I_r A cos\theta_r}{I_i A cos\theta_i} = \frac{I_r}{I_i} \quad (4)$$

In Equation 4, I_r is the reflected flux density, I_i is the incident flux density, A is the cross sectional area of the light, θ_r is the angle of reflectance, and θ_i is the angle of the incident light. The incident and reflected angle of the light are equal and therefore the equation can be reduced to reflected power over incident power. When measuring the reflectance, the incident light will remain constant and therefore, the reflectance of the material is directly related to the fluctuation of the reflected power.

By using a PCM as the sample, the reflectivity of the device can be altered as the material undergoes a phase transition. Raux *et al.* showed that for GeTe, the reflectivity fluctuates up to thirty percent when it crystallizes [14]. This large change in reflectance

can be used in a variety of reconfigurable devices. By knowing the transition temperature of the PCM, an optical temperature monitor can be created. Once the material reaches the temperature required to generate a transition, the reflectance of the material will alter significantly. If the PCM has a nonvolatile transition, it will need to be melt-quenched in order to reset the sensor. However, if the transition of the PCM is volatile, the reflectance will revert back to its initial value as soon as the sample drops below the transition temperature. This can also be extremely useful in monitoring the state of a PCM used in a reconfigurable circuit. By only measuring the optical properties of the sample, there is no need to invasively monitor the resistivity of the device in order to determine which state the PCM is in.

The change in reflectivity that occurs when the PCM transitions can also be used to create an optical switching device. Using a configuration similar to Figure 5, the PCM sample will act as the switching component. With the photodetector threshold set to a level in between the power reflected from the PCM in a crystalline state and an amorphous state, an optical switch can be created. By changing the state of the PCM, the photodetector will produce either an on or off signal. With no intermediary states, the PCMs will always provide a true on or off signal when used as an optical switching component. In addition to these switching mechanisms, PCMs can also be utilized in MEMS based micro-switches.

2.2.3 Reconfigurable MEMS Devices

Many MEMS devices utilize cantilevers in a variety of applications such as micro-switches, resonators, and accelerometers [15]. The operational characteristics of

each of these devices are dependent on the spring constant and geometries of the cantilever. In most devices the geometries of the device are fixed during fabrication and therefore, the spring constant must be reconfigurable in order to create tunable MEMS devices.

The spring constant, k, of a rectangular cantilever can be calculated by

$$k = \frac{Et^3w}{4l^3} \quad (5)$$

where E is the Young's modulus of elasticity, t is the thickness, w is the width and l is the length of the cantilever [16]. By incorporating PCMs into the cantilevers, the Young's modulus can be reconfigured as the device undergoes a phase transition. This will enable many different MEMS devices to be tuned without mechanically altering the cantilever configuration or geometries.

Cantilevers can be used to make micro-resonators that can be used in a variety of applications including RF signal filtering [17]. The resonant frequency of the rectangular cantilever can be found using Equation 6:

$$f = \sqrt{\frac{k_n^4}{12}}\left(\frac{h}{L^2}\right)\sqrt{\frac{E}{\rho}} \quad (6)$$

where L is the length of the cantilever, h is the thickness of the beam, E is the Young's modulus, ρ is the density of the material, and k_n is the first order resonance of the device. When the PCM cantilever undergoes a phase transition, the resonant frequency will change proportionally to the change in the Young's modulus. This allows for MEMS resonators to be repeatedly reconfigured *in situ*.

These cantilevers are also used in electrostatically actuated micro-switches. It is important that the cantilever has a large spring constant in order to prevent it from being stuck down when actuated. However, by increasing the spring constant and restoring force of the cantilever, more voltage is required to actuate the switch. The pull-in voltage required to close the switch can be calculated using Equation 7:

$$V_P = \sqrt{\frac{8kg_o^3}{27\varepsilon_o A}} \tag{7}$$

where k is the spring constant defined in Equation 5, g_o is the initial gap between the cantilever and the actuation pad, ε_o is the permittivity of free space, and A is the area [18]. When the PCM cantilever has a low Young's modulus, the micro-switch will require less voltage to actuate than when the PCM is transitioned to its alternate state. Depending on which PCM is used for the cantilever fabrication; the change in the Young's modulus may be volatile or non-volatile. Similar to traditional micro-switches, PCM based switches may also face durability issues.

2.3 Micro-switch Reliability

Micro-switches are commonly used in a variety of DC and RF MEMS applications. Some examples of these applications are phase shifters, impedance tuners, and filters that can be found in communication and radar systems [19]. Figure 6 shows an example of an electrostatically actuated micro-switch. When these switches are actuated with the circuit on, their lifetime has been reported as 10^7 cycles [4].

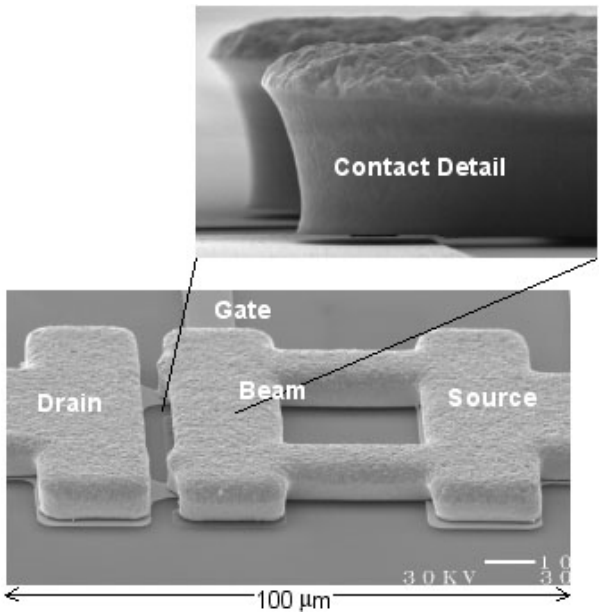

Figure 6. Electrostatic micro-switch [20].

Failure of these switches has been attributed to stiction, fretting, material transfer as well as other mechanical and electrical failure modes. By removing the mechanical component of a micro-switch, the lifetime of the switching component will be drastically increased.

2.4 Germanium Telluride as a Micro-Switch Component

In order to remove the mechanical component of a micro-switch, a GeTe wire may be used because the resistivity of GeTe drastically varies depending on the state it is in. While amorphous, it has an average resistivity of $10^{2}\Omega$-cm, but when it is crystallized, its resistivity decreases up to six orders of magnitude to $10^{-4}\Omega$-cm [21]. Once each phase, is achieved, no additional power is required to maintain it. The large variance in resistivity, low power transitions, and lack of a mechanical component make GeTe a possible micro-switching component.

Chua *et al.* fabricated a GeTe based switching on a silicon substrate with 1 μm of thermal oxide [21]. Figure 7 shows the completed PCM micro-switch component. A 500nm copper (Cu) bottom electrode was first deposited on a 50nm TiW adhesion layer. Then, the 100nm GeTe pillar was then deposited between two silicon dioxide (SiO_2) pillars.

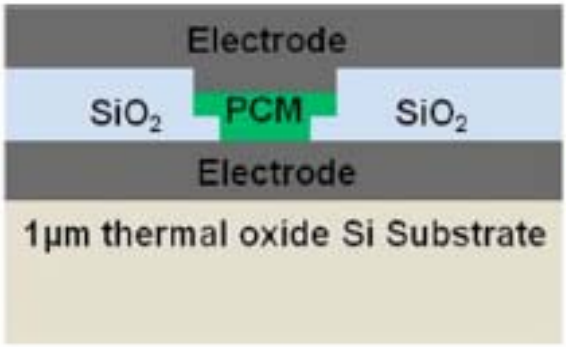

Figure 7: Structure of GeTe based micro-switching component with copper electrodes [21].

The SiO_2 served as an electrical isolation layer for the PCM switching component. Lastly a Cu top electrode was deposited to complete the design. All layers were sputter deposited and patterned using photolithography and lift-off patterning.

To transition the material, a square voltage pulse with a 5ns rise/fall time was used. By adding a resistor in series, Chua *et al.* were able measure the voltage drop and calculate the current flow through the PCM circuit [21]. The additional resistor also allowed another way to control the amount of current that passed through the GeTe layer. The resistance of the PCM was then calculated using Equation 8:

$$R = \frac{V_{applied} - V_{R_s}}{I} \quad (8)$$

where V_{Rs} is the voltage drop across the resistor and I is the current calculated to be passing through the entire circuit. Using this calculated resistance, the state of the material could be determined.

By applying a 1.5V pulse with 16.4mA of current, the switch was transitioned to a "SET", or crystalline, state. In order to reamorphize the GeTe layer, a 5V "RESET" pulse with a current of 57.6mA was used. This higher current was needed in order to heat the material enough to melt-quench it. In order to determine the current required to melt-quench the material, Chua *et al.* derived the formula shown in Equation 9:

$$I_{Reset} = \sqrt{\frac{4\Delta T_{melt}}{R_{th}R_{ON}}} \quad 9$$

where ΔT_{melt} is the melting temperature of GeTe (725°C) minus room temperature, R_{th} is the effective thermal resistance given by Equation 10, and R_{ON} is given by Equation 11.

$$R_{th} = \frac{l}{Ak_{th}} \quad 10$$

The effective thermal resistance represented by Equation 10 is a function of the length and area of the device, as well as the thermal conductivity, k_{th}, of crystalline GeTe (5.65W/m K). R_{ON} in Equation 11 is the resistance of the switch when it is in the SET state and is a function of the resistivity of crystalline GeTe ($4x10^{-4}\Omega$-cm) as well as the device geometries.

$$R_{ON} = \frac{\rho_{ON} l}{A} \quad 11$$

In order to verify the analytical calculations for the RESET current, increasing current pulses where passed through the GeTe component in an attempt to transition it.

Figure 8 shows the results of applying different currents with a 50Ω and a 1000Ω resistor in series with the switching component. The analytical model matched closely with the results of these tests.

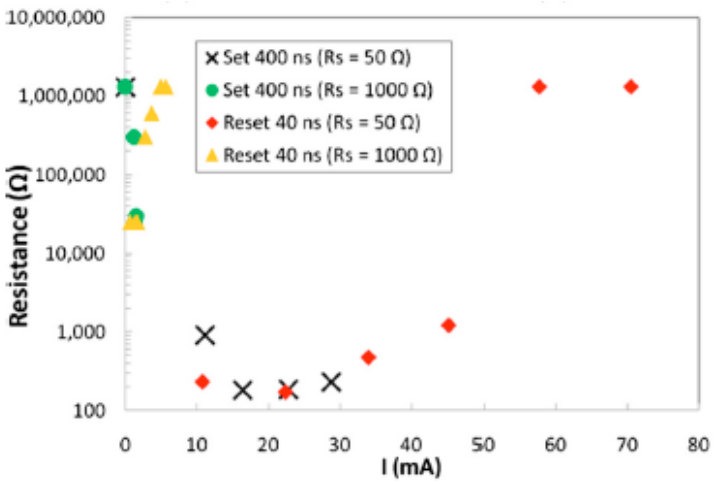

Figure 8: Resistance of GeTe based switch vs. pulse current applied using 400ns SET pulse and a 40ns RESET pulse [21].

2.5 Germanium Telluride as a Phase Change Memory Component

In addition to a micro-switching component, GeTe is also a common chalcogenide material used as a phase change memory component [22]. Its ability to rapidly transition from an amorphous state to a crystalline state, and back, make it ideal for memory applications. With a relatively high crystallization temperature of 180°C, GeTe has the ability to hold its state for longer periods of time in higher temperature environments [23, 24]. The crystallization and subsequent melt-quench processes of GeTe have been performed using two different methods; direct laser pulses, and applied voltage pulses to heaters in direct contact with the GeTe layer.

2.5.1 Crystallization Mechanism of GeTe

PCMs, including GeTe, have been separated into two classes by their crystallization mechanism [25]. In growth dominated crystallization, amorphous regions transition as the crystalline phase grows out from the amorphous region boundaries [26]. The other transition mechanism is nucleation dominated crystallization. In this mechanism, small crystalline nuclei are formed within the amorphous region, and eventually transition the entire spot into a crystalline material. Since nucleation crystallization is not dependent on a bordering amorphous region, the amorphous spot size is irrelevant. On the contrary, growth dominated crystallization is very dependent on the size of the amorphous spot that is being transitioned. This spot size is a direct result of the laser used to generate the phase transition.

2.5.2 Laser Pulse Phase Transition

Using 70mW laser pulses, Bastard *et al.* was able to introduce amorphous spots into crystallized GeTe [23]. These class 3b laser pulses had a duration of 160ns and a wavelength of 504nm [27]. Each pulse created an average amorphous spot size of 366nm. The amorphous spots were then crystallized using thermal annealing. Using transmission electron microscopy (TEM), it was seen that the crystallization mechanism was dominated by growth along the crystalline/amorphous boundary. The growth during the crystallization process can be plotted using the Arrhenius law characteristics of the grain growth given by Equation 12:

$$\ln(u) = -\frac{E_u}{k_B T} + C \qquad 12$$

where u is the growth velocity, E_u is the activation energy for growth, k_B is Boltzmann's constant, T is the crystallization temperature, and C is an arbitrary constant [28]. The continual growth during the crystallization process may eventually create voids near the heat source in the thin film. These voids alter the density of the material and after 10^7 crystal/amorphous cycles may lead to device failure [23].

Raoux *et al.* also used laser pulses to transition GeTe, but his experiments focused on the affects of PCM thin film composition on the transition characteristics [14]. GeTe amorphous films were deposited by co-sputtering elemental Ge and Te sputter targets. By varying the power applied to the sources, 30nm thick films were formed with Ge fractions ranging from 30% to 70%. Studies were then done using a laser with a wavelength of 658nm to determine the power and duration of a pulse needed to crystallize the material. By measuring the reflectivity of the laser, it could be determined exactly when the material crystallized. Figure 9 shows the change in reflectivity as a function of laser power and pulse width for a sample with 41.5% Ge. Each pixel represents a different spot hit with the laser. It is important to note that nearly all the pulses led to either full crystallization or no crystallization at all.

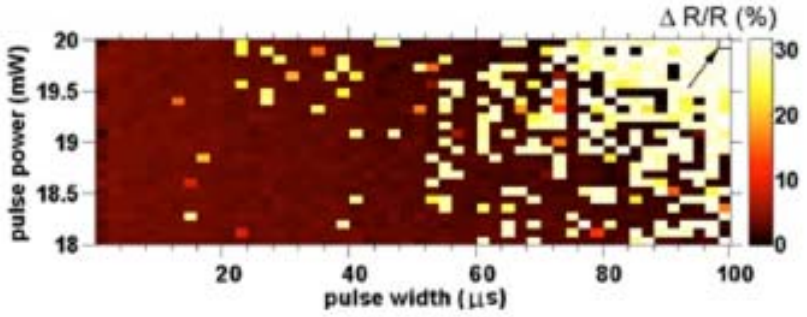

Figure 9: Reflectivity as a function of laser power and duration on an amorphous GeTe film with 41.5% Ge [14].

The arrow in the upper left hand corner of Figure 9 shows the spot measured by the probing laser with an exposure of 20mW for 100μs.

In order to determine the crystallization temperature of the different GeTe compositions, resistance measurements were taken using a custom made setup which used two probes in contact with aluminum (Al) pads on top of a GeTe layer [14]. The crystallization temperature was found to be 180°C for the stoichiometric alloy and up to 350°C for the 72.4% Ge film. To create a uniform crystalline film, the samples were then heated 30°C above their respective crystallization temperatures. These films were then exposed to a variety of laser pulses in order to determine the correct power and duration needed to melt-quench the material. A 100ns pulse of 30mW was found to be ideal for melt-quenching the 41.5% Ge film.

The amorphous spots were then exposed to more laser pulses in order to determine the difference in crystallization parameters of the as-deposited films versus the melt-quenched films. It was found that while the power needed to crystallize the material was similar in both experiments, the time needed to crystallize the film was much less in the melt-quenched samples. This can be attributed to more amorphous-crystalline boundaries near the laser spot which enable faster growth dominated crystallization. Figure 10 shows the difference in the crystallization time of as-deposited and melt-quenched films as a function of the GeTe composition. For certain compositions, the time required to crystallize the film is over two orders of magnitude less for the melt-quenched sample, with the stoichiometric film having the shortest time for both samples. While the crystallization parameters for GeTe will vary with the substrate material and the film thickness, GeTe does show viable properties for use as a phase change material.

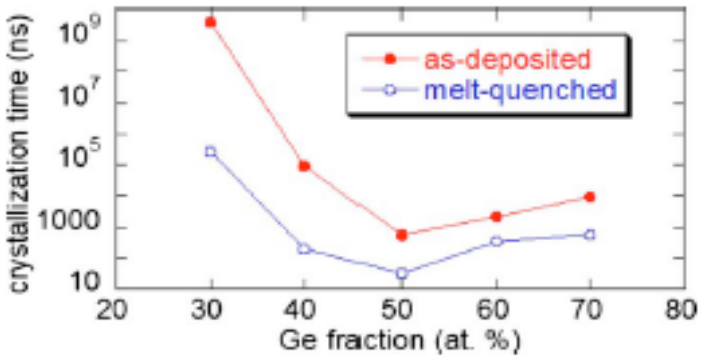

Figure 10: Crystallization time of GeTe films as a function of their composition [14].

Laser pulses have also been used to transition Indium (In) doped GeTe films [29]. The 200 nm PCM films were deposited using thermal evaporation onto p-type Si. The amorphous to crystalline phase change was done using a nanopulse laser with a beam diameter less than 2µm and a wavelength of 658nm. Despite being a doped PCM, the GeTe based film still demonstrated a fast crystallization time as well as a drastic difference in the resistivity between the amorphous and crystalline states. As in the previous example, the reflectance of the film was used to determine its phase. While pure GeTe required a somewhat specific power and duration of a laser pulse to transition, the In dopant allowed the transition to occur with a much wider range of laser pulses. Figure 11 shows the reflectance of the $(InTe)_{0.1}(GeTe)$ film as a function of the laser power and duration. Similar to the results of Raoux *et al.*'s experiment, nearly all the spots hit with the laser either fully crystallized or did not crystallize at all as can be seen by the steep slope shown in Figure 11. The use of lasers to crystallize and subsequently melt-quench GeTe layers is in its simplest form a series of heating and cooling steps. This can also be achieved using methods of heating other than laser pulses.

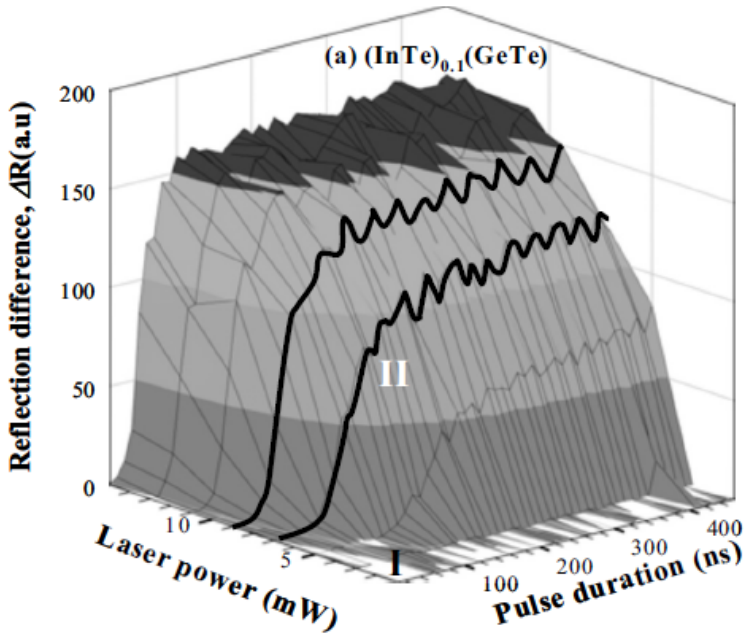

Figure 11: 3-D mesh plot for the reflection of In doped GeTe film as a function of laser power and pulse duration [29].

2.5.3 Phase Transition Generated by a Current Pulse

GeTe based PCM devices can be transitioned from a crystalline phase to an amorphous phase by applying varying strength and length voltage pulses across the material or across a heater in direct contact with the GeTe layer. For use as phase change memory, small single memory cells are fabricated using surface micromachining techniques [3]. These cells are comprised of a bottom electrode (BEC), a Tungsten (W) pillar, a phase change layer, and a top electrode (TEC). Figure 12 shows a schematic of an individual memory cell.

The 300nm wide W pillar is used to heat the GeTe PCM layer above it [3]. The top and bottom electrodes are used to measure the cell resistance, which is directly related to the phase of the GeTe layer.

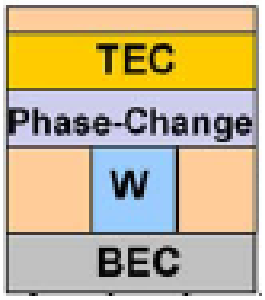

Figure 12: Single phase change memory cell [3].

The electrodes are 20nm TiN layers, which are used for their good electrical conductivity. Each memory cell goes through a 200°C thermal annealing process to establish the device in its SET, or crystalline state. In order to transition the material, voltage pulses are applied to the W pillar. The current that passes through the pillar heats the phase change layer above. The heating will crystallize or melt-quench the GeTe depending on its current state and the amplitude and duration of the pulse applied. For the memory cells shown in Figure 12, a 30ns RESET pulse that generated 30mA of current through the pillar was applied. This amount of current was the minimum required to heat the GeTe layer past its melting point. By using such a short pulse duration, the melted material then rapidly cooled, quenching it back to an amorphous state. The SET pulses for these cells were also 30ns in duration, but by applying only 18mA, the material crystallized but never reached a temperature high enough to melt-quench it.

The endurance characteristics of these memory cells were also explored by Perniola *et al.* After 10^5 cycles, some of the GeTe cells showed signs of not fully crystallizing to their original state. This may be due to voids in the layer being formed during the crystallizing and subsequent melt-quenching process. Figure 13 shows

endurance testing done on two different GeTe cells. The difference between the two graphs may be attributed to slight differences in the layer thicknesses or in the number of voids formed during the transition processes. However, in both cells four orders of magnitude difference in resistance can be seen from a SET to a RESET state. This drastic variation allows for a clear distinction between the memory states.

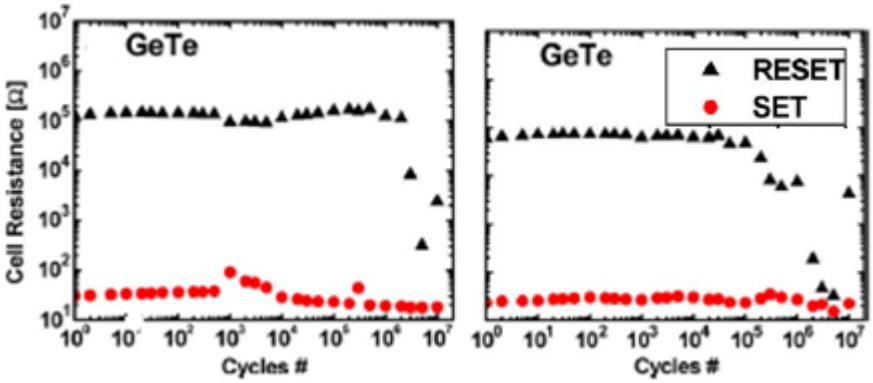

Figure 13: Endurance characteristics for two GeTe memory cells using 30ns SET/RESET pulses with I_{RESET} = 26mA and I_{SET} = 18mA [3].

Using a similar fabrication process to [3], Pashkov *et al.* created memory cells using GeTe as the PCM component [30]. However, these GeTe layers were formed by co-sputtering from Ge and Te elemental targets. By varying the power applied to each sputtering target, the Ge fraction in different cells varied from 30% to 70%. While the amount of current necessary to transition these memory cells is relatively similar for the different GeTe compounds, the resistance of the cells does change up to two orders of magnitude based on the Ge percentage. Figure 14 shows the first RESET current pulse being applied to a device in the SET state. Again it can be seen that the material goes from entirely crystalline to entirely amorphous with only a slight increase in the RESET current.

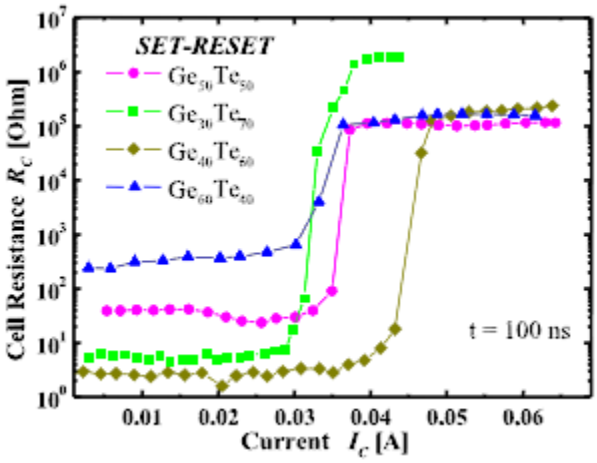

Figure 14: 100ns RESET pulse of increasing current being applied to various GeTe alloys [30].

For these memory cells, 100 ns RESET pulses and 50 ns SET pulses of different amplitudes were used. The RESET pulses had a rise and fall time of 10 ns, creating a quick temperature variation in the cell which caused the GeTe layer to be melt-quenched. After being cycled 10^7 times, the memory cells showed no signs of void formation.

Other research efforts have also shown that GeTe based phase change memory cells demonstrate switching capabilities by using a bottom heater configuration [26, 31]. The 60 nm titanium nitride (TiN) heater is embedded in an isolating silicon nitride (Si_3N_4) layer. This Si_3N_4 layer helps keep the memory cells separate from each other. On top of the heater and insulating layers, a 20 nm thick GeTe layer was sputter deposited as the PCM layer. Lastly, a 20 nm TiN top electrode layer was sputter-deposited and patterned using a lift-off process. The phase change material was then heated to 250°C to crystallize it, resulting in an individual memory cell resistance of 3kΩ.

Current pulses ranging from 1-16ns were applied to the heater [26]. For currents between 400μA and 1.1mA, all memory cells were successfully transitioned to a SET

state. However, the longer the pulse, the lower the resistance of the cell was when in the crystalline state. For all currents above 1.2mA, the memory cells transitioned into a highly resistive RESET state.

Bruns *et al.* demonstrated that a recrystallization speed of 1-5ns can be achieved in GeTe based memory cells using a local heater [26]. This is much faster than the30 ns laser induced recrystallization time that has been reported [25, 32]. This may be attributed to the size difference between laser diameters, around 1μm, and the diameters of the heaters used, 40nm.

2.5.4 Doping of GeTe

Whether using heaters or lasers to generate a phase transition in Germanium Telluride, a semiconductor material, a variety of dopants can be added to alter its material properties. The transition characteristics have also been tuned by altering the alloy stoichiometry [33]. Not only due these alterations to the GeTe layer affect its resistivity in both crystalline and amorphous states, but it also affects the transition speeds and the stimuli required to generate the transitions.

In Sang-Jun Choi *et al.*'s research involving PCM based memory, copper (Cu) was added to the GeTe layer in order to create a multibit phase change memory operation [34]. The addition of Cu allowed multiple set voltages to be used to create partially amorphous or crystalline sections of the PCM. In order to diffuse Cu into the GeTe layer, a 30 nm layer was deposited as the bottom electrode on a SiO_2 insulating layer. By applying a bias to this electrode while sputtering the GeTe, the copper atoms diffused into the layer without having to apply an additional thermal process. During this research

effort, it was noticed that Cu bridges were forming from the top electrode (Tungsten) to the bottom electrode (Copper) as shown in Figure 15. The length and area of these bridges also aided in the formation of multiple resistive states within the CuGeTe layer.

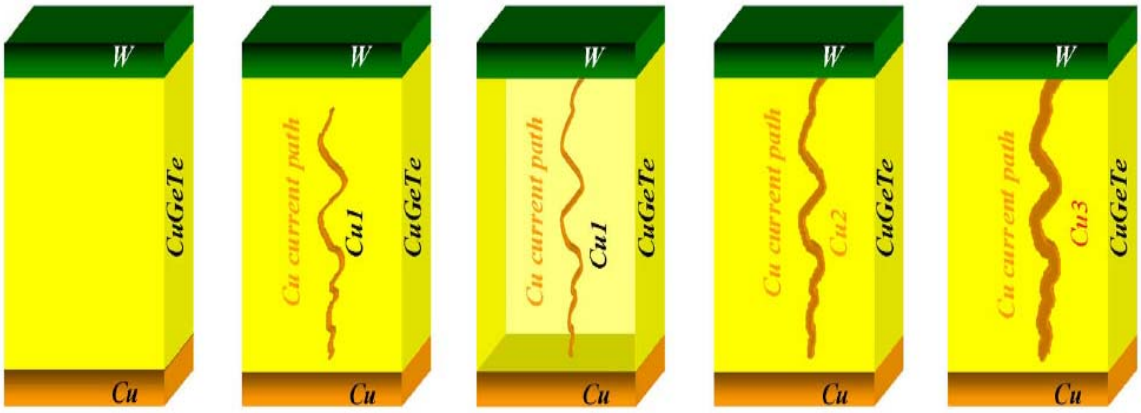

Figure 15: Cu Bridges forming during Set function in CuGeTe thin films [34].

Copper was also introduced to GeTe in order to alter its transition properties by Sutou *et al.* [35]. It was found that the crystallization temperature of $Ge_1Cu_2Te_3$ was around 235°C, which is roughly 55°C higher than that found in literature for GeTe [23]. During their study of phase change memory materials, Sutou *et al.* compared the Germanium Telluride and Copper (GCT) alloy to the well know PCM $Ge_2Sb_2Te_5$ (GST). Figure 16 shows the resistance of GCT and GST as each material is heated. GCT has a much higher crystallization temperature than GST as well as a much lower resistance when in an amorphous state.

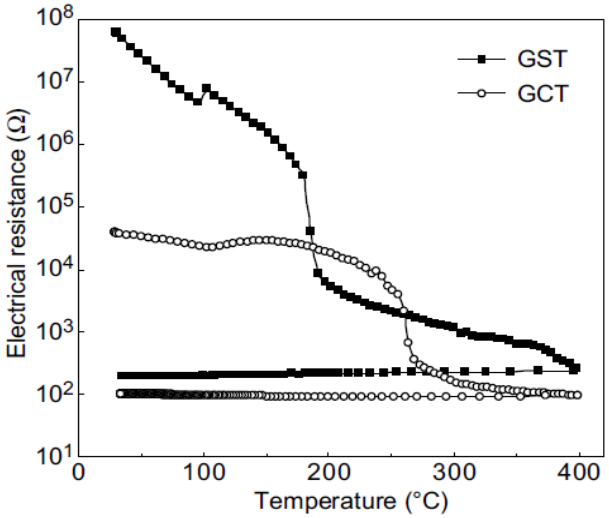

Figure 16: Temperature dependence of the electrical resistance in GCT (Germanium Copper Telluride) and GST (Germanium Antimony Telluride) thin films [35].

To create similar memory test devices, each of the PCMs sputter deposited from single alloy targets of GCT and GST respectively. Each of the PCM layers was deposited between separate Ti and Al electrodes that were used to transition the material. By applying a short voltage pulses to these electrodes, small amounts of current are passed through the PCM, transitioning it from an amorphous state to a crystalline state and vice versa. In order to transition both memory devices into a crystalline state, a 50µs pulse was applied to the electrodes at increasing voltages. Similarly, a 5µs pulse of increasing voltage was applied to reset the device back to an amorphous state.

For phase change memory applications of PCMs, the crystallization time is very important. The time t_e that it takes to reach a crystallization percent x at a given temperature T_i is show by Equation 13 [35]:

$$t_e = \theta_n \exp\left(\frac{E_a}{RT_i}\right) \qquad 13$$

where E_a is the activation energy, R is the gas constant around the material, and θ_n is a reduced time coefficient. When the sample is being heated at a constant rate, θ_n is given by Equation 14 [35]:

$$\theta_n = \frac{E_a}{\beta R} p(\frac{E_a}{RT_n}) \quad 14$$

where β is the heating rate and T_n is the temperature at which x amount of the material is crystallized.

In order to tune the transition properties of GeTe based devices, Silver (Ag) has also been used as a dopant. Lee *et al.* conducted research in which Ag was added to GeTe amorphous films for phase change memory applications [36]. In order to create the AgGeTe alloy, Ge and Te targets were used in RF magnetron co-sputtering. Different powers were used with each to get different ratios of Ge and Te for testing purposes. A 300 nm silver layer was then sputter deposited on top of the GeTe layer. During this deposition process, at room temperature, the Ag diffused into the GeTe layer, as confirmed by x-ray photoelectron spectroscopy (XPS). The samples with a higher Te concentration increased the amount of Ag that was diffused into the GeTe layer. Tungsten (W) electrodes where used on either side of the AgGeTe devices in order to transition the material. By doping the 200nm thick film with Ag, the crystallization temperature was increased to 250°C and the sheet resistance changed to $10^7\Omega/\square$ for amorphous films and $10^2\Omega/\square$ for crystalline films [36].

Kim *et al.* also used Ag as a dopant in GeTe for nonvolatile random access memory applications. He created an AgGeTe ternary alloy by RF magnetron tri-sputtering Ag, Ge, and Te. An Ag anode was then deposited on top of the AgGeTe layer

to supply neutral silver atoms to the AgGeTe layer. After depositing several different ratios of the materials, $Ag_{30}(Ge_{0.3}Te_{0.7})_{70}$ was chosen for memory testing. The 2μm device was transitioned with 0.13V from an "off" state with a resistance of $10^6\Omega$ to an "on" state with a resistance of $10^2\Omega$. Voltage pulses of 1μs were used to transition the material. This material transitioned well for several switching cycles, but eventually failed due to an excess amount of diffusion from the silver anode.

Although not as popular as silver or copper dopants, Indium (In) has been used to alter the crystallization time in GeTe based PCMs [29]. The material was prepared by melting the individual materials together in an evacuated quartz ampoule at 1000°C for twenty four hours. After that time, it was quenched in cold water, creating an amorphous film. The 200nm samples were then deposited using thermal evaporation onto p-type silicon. These Indium Germanium Telluride (IGT) films were transitioned using a nanopulse laser. The crystallization temperature of these films was found to be around 200°C. In Figure 17, the sheet resistance of the IGT films with different In concentrations is shown.

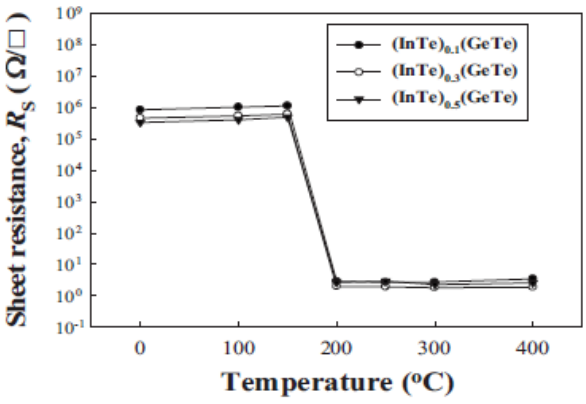

Figure 17. Temperature-dependent sheet resistance for 200nm Indium Germanium Telluride (IGT) films with varying In concentration [29].

The addition of In atoms to the PCM film does not drastically alter the resistivity of the material. However, it does impact the crystallization time. Using the nanopulse laser, Song *et al.* compared the transition times of the IGT films with that of GST films. For the films with small amounts of In dopants (around 1%), crystallization time was faster than that of GST films. This may be attributed to the IGT films crystallizing in a single step, whereas GST films have a two-step phase transition (amorphous to fcc then fcc to hexagonal) [29].

While GST is one of the most common phase change memory materials, it has a relatively low crystallization temperature, making its data retention poor at high temperatures [37]. In order to avoid this fatal flaw in phase change memory, Lu *et al.* used Titanium Dioxide (TiO_2) to dope GeTe [38]. This Ge_2Te_3-TiO_2 was fabricated by co-sputtering independent GeTe, Te and TiO_2 targets at room temperature in an argon atmosphere. Different powers were applied to the TiO_2 target, creating samples with concentrations of 5 and 15% (verified by energy-dispersive X-ray spectroscopy). These compounds had a crystallization temperature of around 250°C. The addition of a 15% concentration of TiO_2 decreased the amorphous resistivity by two orders of magnitude, while increasing the crystalline resistivity by half an order of magnitude as shown in Figure 18. This is attributed to the TiO_2 having a lower amorphous resistivity than GeTe, but a higher crystalline resistivity. The Ge_2Te_3-TiO_2 compound also required less voltage than GST to transition, making it more energy efficient [38].

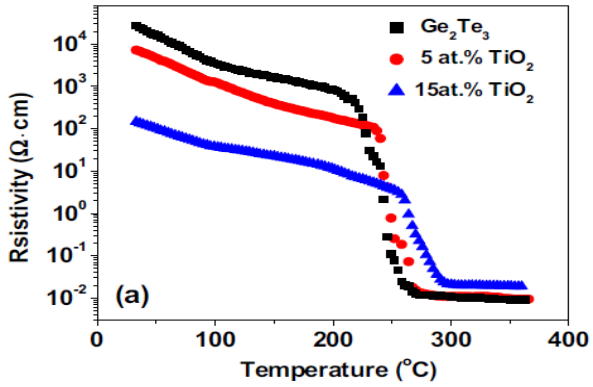

Figure 18: Resistivity of GeTe sample doped with TiO_2 as temperature is increased [38].

Other materials such as Tin (Sn) and Selenium (Se) have been used as dopants to alter the transition properties of GeTe films for phase change memory applications [39, 40]. These two materials reduced the crystallization temperature of the doped GeTe films, allowing for lower power phase change memory applications. In order to alter the magnetic and thermoelectric properties of GeTe films the following materials have been introduced as dopants: Vanadium (V), Chromium (Cr), Manganese (Mn), Lead (Pb), and Iron (Fe) [41, 42, 43, 44]. While these dopants affect the material properties of GeTe, the researchers did not report any information on their affects on the phase change properties. In addition to doped GeTe, other chalcogenide materials also exhibit a variety of phase change characteristics.

2.6 Comparison of GeTe and $Ge_2Sb_2Te_5$ Phase Transition Characteristics

Germanium Antimony Telluride ($Ge_2Sb_2Te_5$) is a very popular chalcogenide material used for phase change memory applications [45]. Research has been done to determine which material, GeTe or $Ge_2Sb_2Te_5$ (GST), is the better for nonvolatile memory applications [37]. The attributes that are used to determine what makes a better

phase change memory material include: crystallization temperature, resistance contrast between states, and crystallization time.

It is important for phase change memory devices to have high crystallization temperatures. This allows them to maintain their states when used in elevated temperature applications such as automotive systems and other high temperature consumer products [37]. Fantini *et al.* reported that the crystallization temperature of GST is only 145°C, while GeTe has a crystallization temperature of 185°C. Therefore, at any temperature above 145°C, GST will not maintain its memory state, while GeTe can operate at temperatures up to forty degrees higher.

GeTe has an abrupt resistance change of approximately five orders of orders of magnitude when it transitions between a crystalline and an amorphous state [37]. This transition is extremely large when compared to only two orders of magnitude change for GST. Figure 19 shows the crystallization of amorphous GST and GeTe samples as a function of temperature.

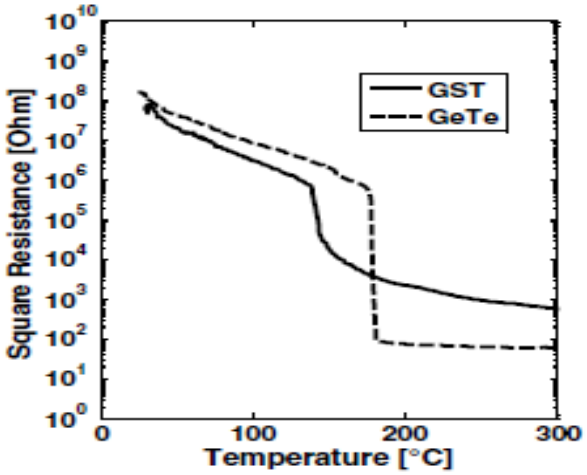

Figure 19: GeTe and GST sheet resistance as a function of temperature with a constant heating rate of 10°C/min [37].

It can also be seen in Figure 19 that GeTe has a sharp change in resistance at its crystallization temperature, while GST has a transition that occurs over a range of temperatures. This adds complexity to GST based phase change memory by adding intermediary resistive states in between the amorphous and crystalline phases.

Using a 30nm thick PCM layer in between a top metallic electrode and a tungsten heater, Fantini *et al.* measured the current necessary to crystallize and melt-quench GeTe and GST [37]. Both materials were tested starting in a SET state as well as starting in a RESET state while an increasing current pulse is passed through the heater. Figure 20 shows the resistance of the GeTe and GST memory devices as a function of the current pulses.

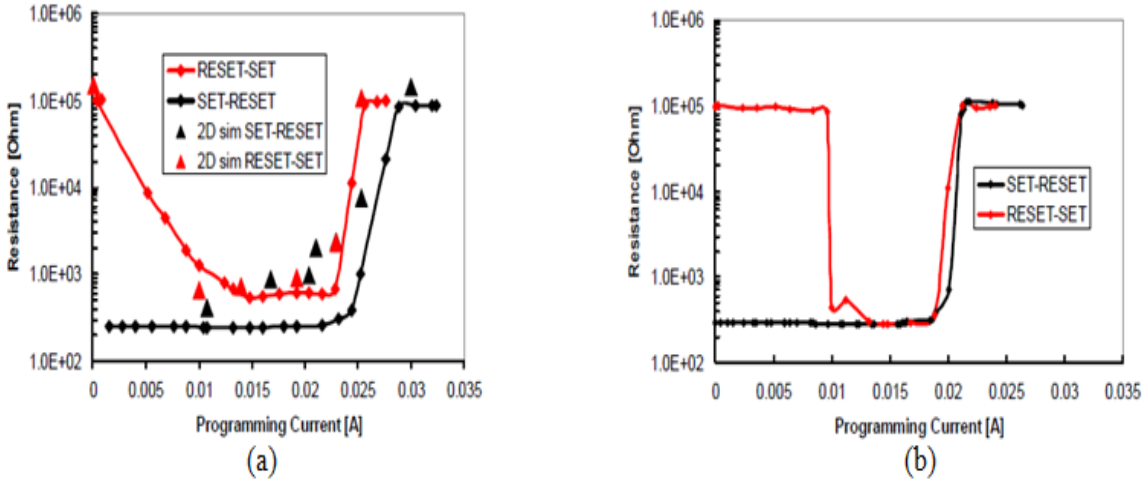

Figure 20: Electrical programming R-I curves measured on (a) a 30nm thick GST layer and (b) a 30nm thick GeTe layer [37].

To transition the material from amorphous to crystalline a 1µs pulse was used. The crystalline to amorphous transition was achieved using a much shorter, 50ns, pulse. The transition in GeTe is much sharper than the GST in both SET and RESET functions.

Due to its higher crystallization temperature, greater difference in phase resistivity, and sharper transition, GeTe has the potential to be a better PCM for phase change memory applications as well as reconfigurable applications than GST. While GeTe is an ideal PCM for many applications, other PCMs such as VO_x exhibit phase change characteristics that can be utilized in reconfigurable applications.

2.7 Vanadium Oxides as PCM

A variety of Vanadium Oxide (VO_x) phases have been studied for their unique phase change properties [46, 47]. Unlike the chalcogenide class of PCMs, VO_x PCMs demonstrate a volatile transition. In addition, this material can be transitioned not only using a thermal stimulus, but also electrical and optical [48, 49]. While many of the VO_x phases have been studied for their phase change properties, Vanadium Dioxide (VO_2) has been the most popular due to its relatively low transition temperature. In order to determine the exact phase of the VO_x films, the reflectance can be measured and compared to known values from literature. Figure 21 shows the reflectance values for V_2O_5, V_6O_{13}, and two samples of VO_2.

At room temperature, VO_2 single crystals have a monoclinic lattice structure and a resistivity of around 20Ω-cm [2]. However, above its critical temperature, 68°C, VO_2 transitions to a tetragonal structure with metallic like behavior and a resistivity of 10^{-5}Ω-cm. In order to measure the resistivity changes in the VO_2 films, Dumas-Bouchiat *et al.* deposited the thin films using pulsed laser deposition (PLD) on sapphire and SiO_2/Si substrates.

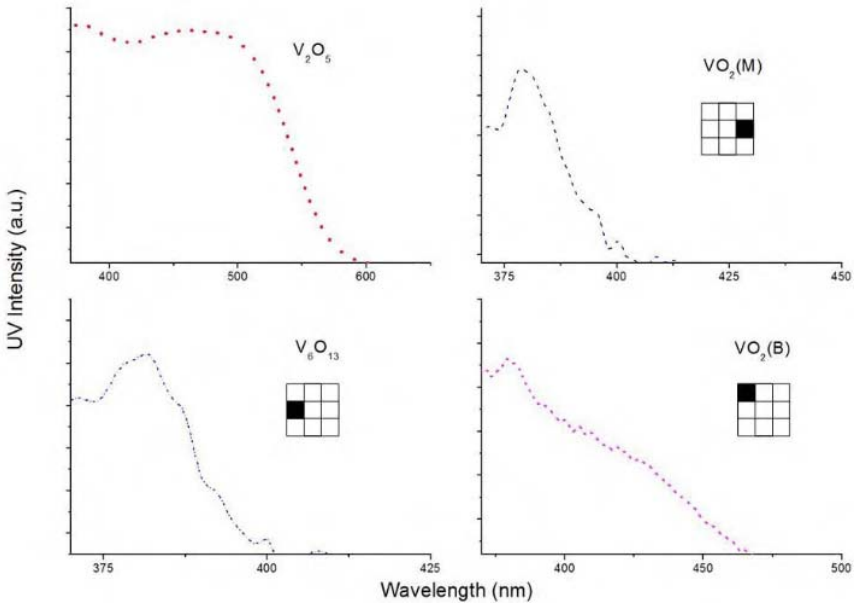

Figure 21: Reflectance spectra of various vanadium oxides [50].

The deposited films were then characterized using X-ray diffraction (XRD). The film on sapphire demonstrated a good monoclinic phase with low lattice mismatch. However, the film on SiO_2 showed significant lattice mismatch but was still in a polycrystalline state.

Both films were then exposed to heating-cooling loops from 27°C up to 102°C while their resistivities were measured [2]. While both films transitioned around the critical temperature, the VO_2 film on sapphire showed a much more drastic variation in resistivity. Figure 22 (a) shows the changing resistivity of VO_2 on the sapphire substrate and Figure 22 (b), the inset, shows the change on the SiO_2/Si substrate.

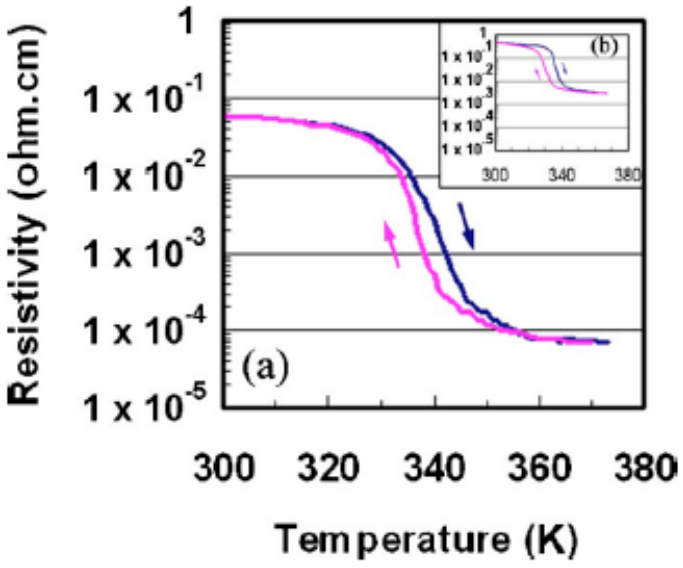

Figure 22: Resistivity vs. temperature for a 200nm thick VO_2 film on: (a) C type sapphire substrate and (b) SiO_2/Si substrates [2].

The dark blue line represents the material being heated, while the pink line represents the material being cooled. Although not mirror images of each other, they do follow very closely. The transition back to a high resistive state when cooled is what sets apart VO_x phases from other PCMs.

While VO_2 has a resistivity too large to be an ideal micro-switch for DC applications, the large variation in resistivity can be extremely useful in tunable RF devices. By using a thin VO_2 layer in the middle of a RF signal line, as shown in Figure 23, a variety of tunable RF devices can be created. Using these VO_2 wire segments, researchers have designed and fabricated micro-switches, tunable band stop filters, microbolometers, and other RF devices [51, 52, 53]. In order to generate the heat necessary to transition VO_2, various heating methods can be used.

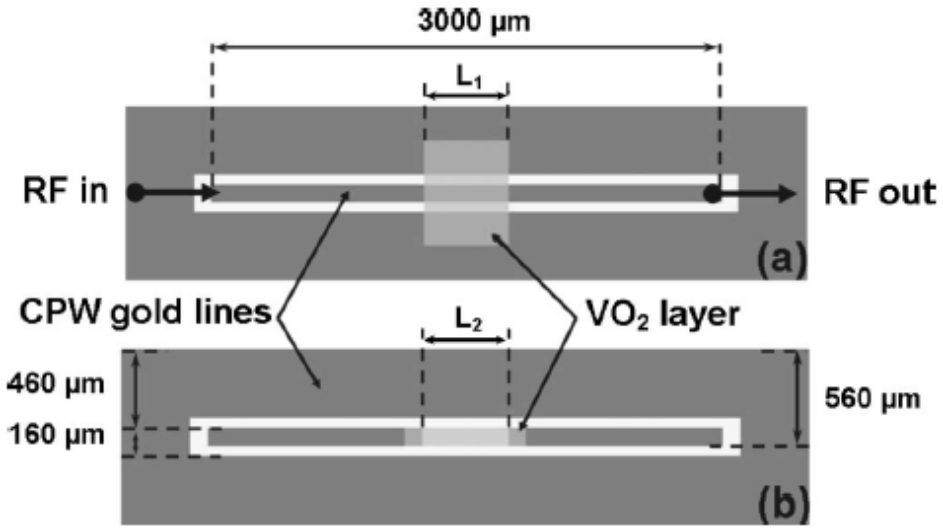

Figure 23: RF switching device using VO_2 thin films as the micro-switching component: (a) shunt configuration and (b) series configuration [2].

2.8 PolyMUMPs Heater Fabrication

Heaters used to transition PCMs can be fabricated in a variety of ways. The Polysilicon Multi-User MEMS Process (PolyMUMPs®) was used by Captain Scott Ostrow to create meandering heaters [54]. This fabrication process consists of the seven layers shown in Figure 24. The first layer deposited is the silicon nitride (Si_3N_4) layer using LPCVD on a <100> oriented, n-type silicon wafer. This layer is used to electrically isolate individual devices from each other. Next, a 500 nm polysilicon layer (Poly0) is deposited using LPCVD. This layer is then patterned using photolithography and plasma etching. After the Poly0 base layer, a series of two sacrificial oxides, 2 µm and .75 µm, and two additional polysilicon layers (Poly1 and Poly2), 2 µm and 1.5 µm, are deposited individually and patterned. Lastly, a .5 µm gold layer is deposited on top of the Poly2 layer. The Poly1, Poly2, and gold are used as structural device layers in the meandering heaters.

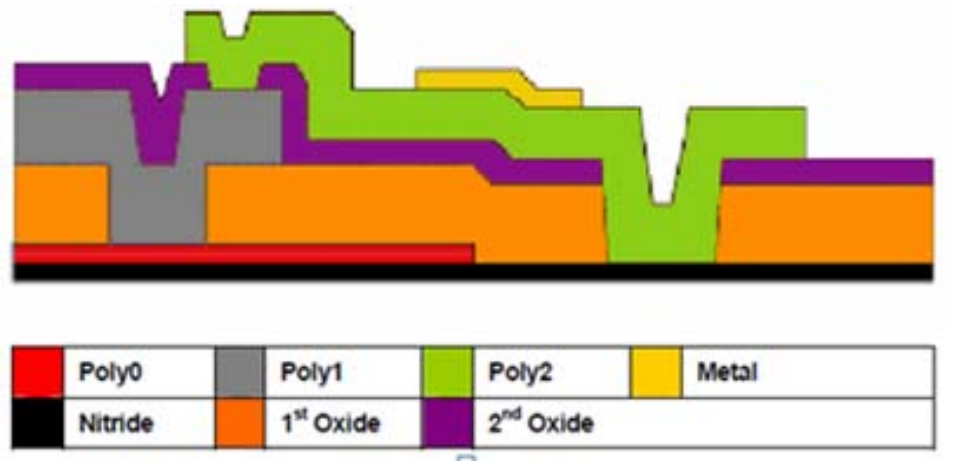

Figure 24: Cross-sectional view of the seven PolyMUMPs layers [55].

2.8.1 Meandering Heater Design

The heaters created by Captain Ostrow utilize meandering resistors to generate heat through Joule heating. He created several different designs, each with different heating abilities. The amount of heat that a resistor generates is a function of its resistance and the amount of current passing through it. The resistance of the heaters created is determined by their length, width, thickness, material and its resistivity [56]. Compared to a straight resistor, the resistance of a meandering resistor is much more difficult to calculate due to the current not passing through the far corners of the device [56, 57]. A calculation based on the PolyMUMPs process of the resistance in a meandering heater is shown in Equation 15:

$$R = \big((b+1)(l-2w) + (b+3)g + (2b+4).6w\big)R_{\square}/w \qquad 15$$

where R is the resistance of the heater, b is the number of arms, l is the length of each arm, w is the width of the arms, g is the gap between the arms, and $R_{\square}$ is the sheet resistance [57]. The sheet resistance, shown in Equation 16, is equivalent to the resistivity of the material divided by its thickness.

$$R_{\square} = \frac{\rho}{t} \quad (16)$$

After fabrication, hydrofluoric acid (HF) is used to remove the sacrificial oxides and leave the polysilicon and metal device layers attached to the substrate only at their anchor points. Figure 25 is an example of a basic meandering resistive heater. Using a micromanipulator, these heaters can be detached from the substrate and moved on top of other devices to heat them.

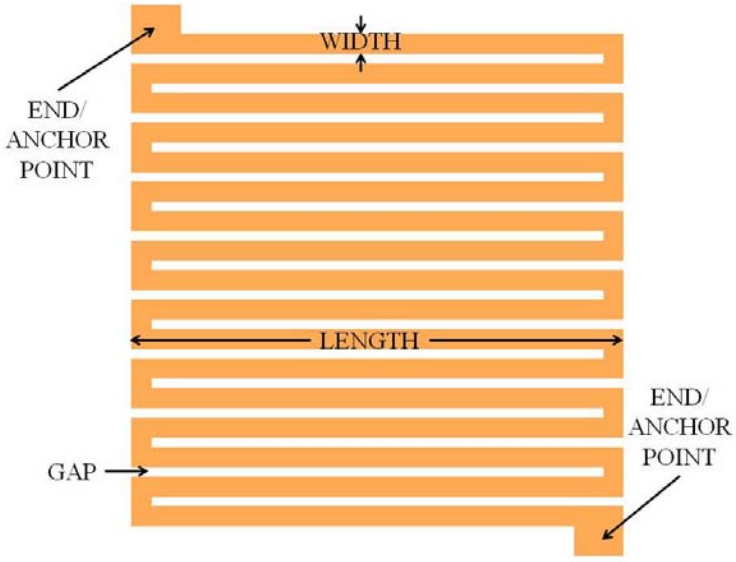

Figure 25: Example of a meandering resistive heater [54].

2.9 Summary

This chapter outlined the background information necessary to move forward in this area of research. Each PCM requires different external stimulus in order to achieve its metal-insulator transition. The different applications these PCMs are capable of being used in is a function of their individual transition characteristics. Chalcogenide PCMs provide the nonvolatile transition capability required for phase change memory and other lower power applications. A variety of VO_x phases have been shown to be ideal micro-

switching components in tunable RF devices. While each of these materials is best fit for a particular application, doping and varying their stoichiometry can be used to fine tune the phase change characteristics of each one. All of the information presented in this chapter will be used in designing the methodology and testing techniques, presented in the next section, which will be used in this research.

3. Methodology

3.1 Chapter Overview

This chapter discusses the methodology for designing, fabricating, and testing novel PCM test structures. In addition, witness samples will be prepared and tested to characterize additional material properties of the PCMs. The test structures created will allow resistance measurements to be taken while applying thermal and electric field external stimuli. Several device designs are being fabricated for both DC and RF testing. While a variety of PCMs can be fabricated within this design, this research effort focuses on GeTe and VO_x. By using a single design to test multiple PCMs, a direct comparison of their switching characteristics can be made. Once the stimuli needed to transition the PCM is known, experiments are tailored to optimizing the stimuli and how it is applied to the material.

3.2 Test Structure Design

The majority of PCM testing done in this research is based on the application of a thermal and/or electric field stimulus. To apply these stimuli, micro-test structures were designed using MEMS Pro L-Edit software and then fabricated in AFIT's class 1000 clean room. With a focus on using the PCMs as micro-switching components or reconfigurable device components, the goal of the structures is to alter the resistivity of the material using a thermal or electric field stimulus.

3.2.1 Thermal Stimuli Test Structure

In order to monitor the resistivity of a PCM while it is heated on a thermal stage, a structure was designed with a PCM layer between two test pads as shown in Figure 26. Various geometries are used in order to determine the effect of device length and area on the transition properties of the PCM. Each sample made contains devices of 200µm, 600µm, and 2,000µm in length and 20µm or 40µm in width.

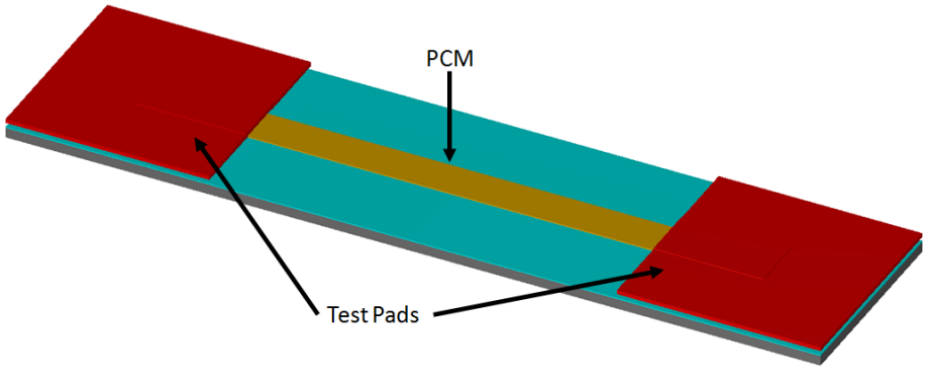

Figure 26: Thermal test structure for PCMs.

3.2.2 Electric Field Stimuli Test Structure

The transition of PCMs has also been induced with the application of an electric field [58]. In order to apply this field across the PCM wire segment, a separate test structure needed to be made. Using two parallel gold wires, 80µm or 100µm apart, a parallel plate capacitor is created around the PCM wire. By applying a voltage differential between the two wires, an electric field is created with a strength based on Equation 17,

$$\mathrm{E} = \frac{V}{D} \qquad 17$$

where E is the electric field strength, V is the voltage difference between the two gold wires, and D is the distance between them. In order to make probing the device easier, test pads were added to the design as seen in Figure 27. The electric field test structures were fabricated in lengths of 200µm, 600µm, and 2,000µm, with widths of 20µm, and 40µm. By making the PCM wires identical for both the thermal and electric field test structures, a direct comparison between the two stimuli can be made.

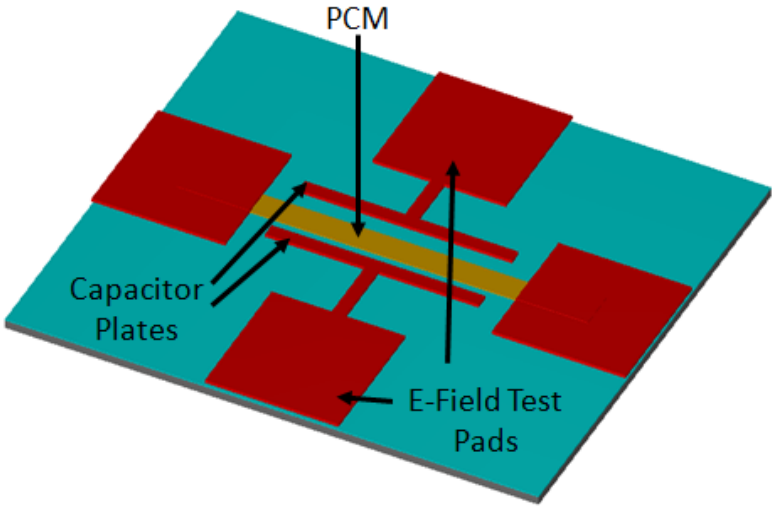

Figure 27: Electric field test structure for PCMs.

The test pads on each end of the PCM wire are used to measure its resistance. Then using Equation 18, the resistivity of the material can be calculated.

$$R = \frac{\rho L}{A} \quad 18$$

In Equation 18, R is the resistance across the PCM material, L is the length of the wire segment, A is the cross-sectional area of the wire segment, and ρ is the resistivity of the material. During the testing of PCMs, the geometries of the device will remain constant while the external stimuli are applied in an attempt to alter ρ.

3.2.3 RF Test Structure

While the designs described above are ideal for testing the DC phase transitions in a variety of PCMs, a separate device needed to be made to test the RF properties of these materials. The RF probe stations used at AFIT are equipped with ground-signal-ground probes in order to better isolate the signal line from noise. These probes are connected to a programmable network analyzer (PNA) in order to measure the S_{21} and S_{11} signals through the PCM wire. In order to accommodate the ground lines, additional pads had to be added above and below the PCM wire segment. For the thermal test structures, these ground lines could be easily added. However, in order to electrically isolate the parallel gold wires from the ground lines, a dielectric had to be added in between them. This is shown as the grey layer in Figure 28.

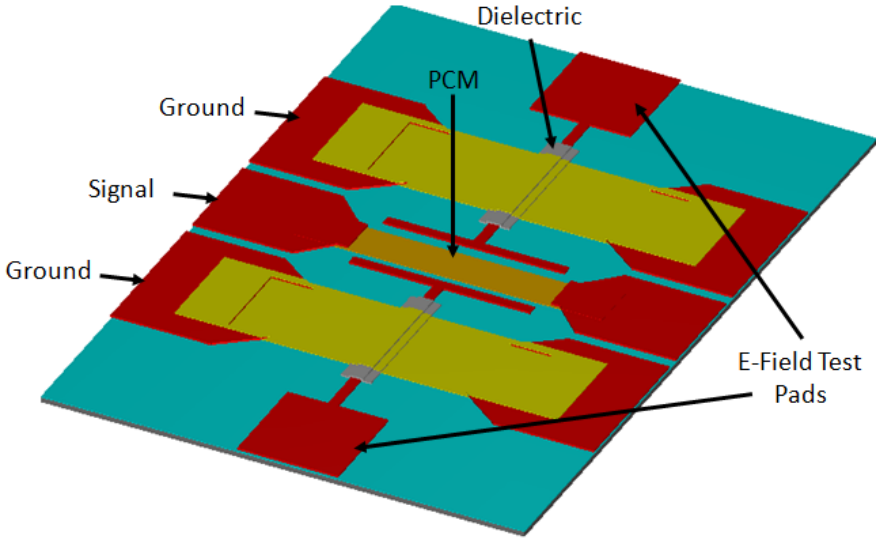

Figure 28: RF electric field test structure for PCMs.

3.3 Test Structure Fabrication

During this research effort, the test structures described above were fabricated for testing VO_x and GeTe. Both materials were fabricated in the DC and RF test structures

described above. The DC and RF structures require the same two initial layers, but the RF structures require two additional device layers. In order to utilize the entire three inch mask, all four layers were written on one mask.

The devices are fabricated on two different substrates, <100> Silicon with a native oxide and <100> Silicon with 600nm of silicon nitride (Si_3N_4). The nitride layer is used to electrically isolate the devices. Each of the three inch wafers were cleaved into four quarter wafer pieces so that they will fit under each of the quadrants of the mask. Each wafer piece then went through the fabrication process individually and included RF and DC test structures as shown in Figure 29. The green and purple colors on the substrate are the Si_3N_4 electrical isolation layer.

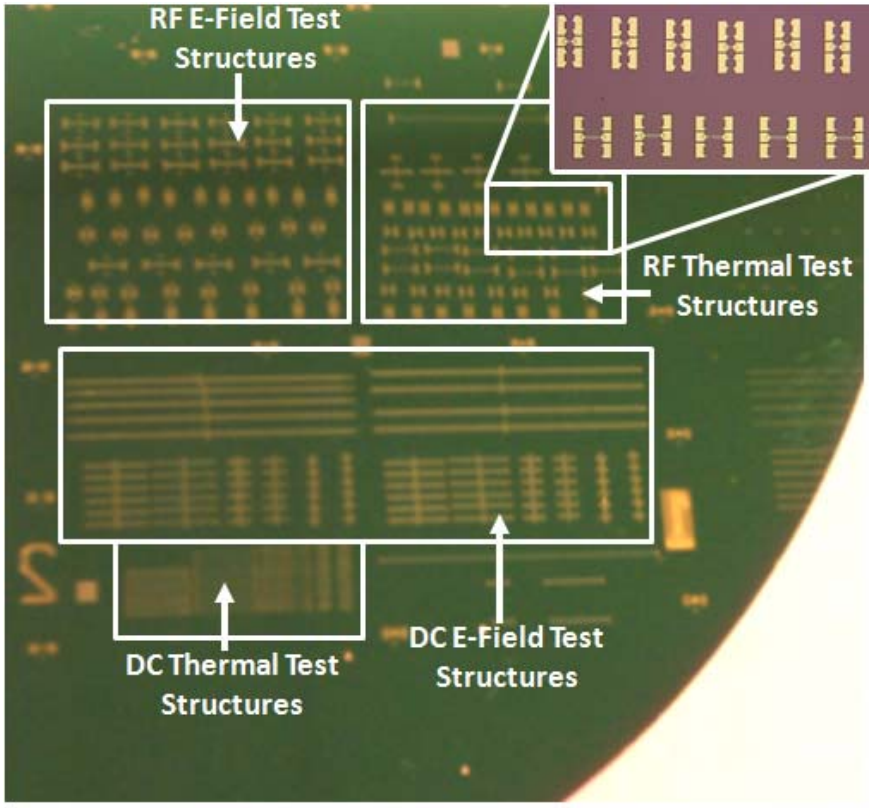

Figure 29: Quarter Si wafer with 600nm Si3N4 layer and PCM test structures.

After cleaving the wafers, the samples were cleaned with a series of acetone, methanol, isopropyl alcohol, and DI water sprays while rotating at 500rpm. A dehydration bake was then done to remove any remaining solvents from the surface of the wafer. To pattern the PCM on the wafers, SF-11 photoresist was spun on the wafer for 30 seconds at 4,000rpm. The resist was then baked for two minutes at 200°C to make it more robust. After baking, the wafer was coated with 1805 positive photoresist for 30 seconds at 4,000rpm, followed by an additional post bake of 75 seconds at 110°C. These two layers of resist provide the necessary height for the deposited PCM to be patterned using lift-off.

The samples were then exposed to UV light through the first mask. After developing the 1805 photoresist, small trenches were formed which exposed the SF-11 where the PCM segments go. A deep UV source was then used to slightly overexpose the SF-11 resist in the trenches. The overexposure is necessary to create a small lip under the 1805 layer that will enable the deposited PCM wires to be lifted-off. After developing the SF-11, the samples were placed in the oxygen plasma asher for five minutes to remove any residual resist.

The PCM is then deposited on the wafer using RF magnetron sputtering. The GeTe samples were sputtered from a single GeTe target with a composition of 50% germanium and 50% tellurium. The VO_x samples were made by sputter depositing 99.99% pure vanadium and then oxidizing the sample after the deposition. The desired thickness of the PCM is 200nm so that it is closely impedance matched to the network analyzers used for RF testing. Figure 30 (a) shows an illustration of the MIT material deposited on top of the photoresist layers.

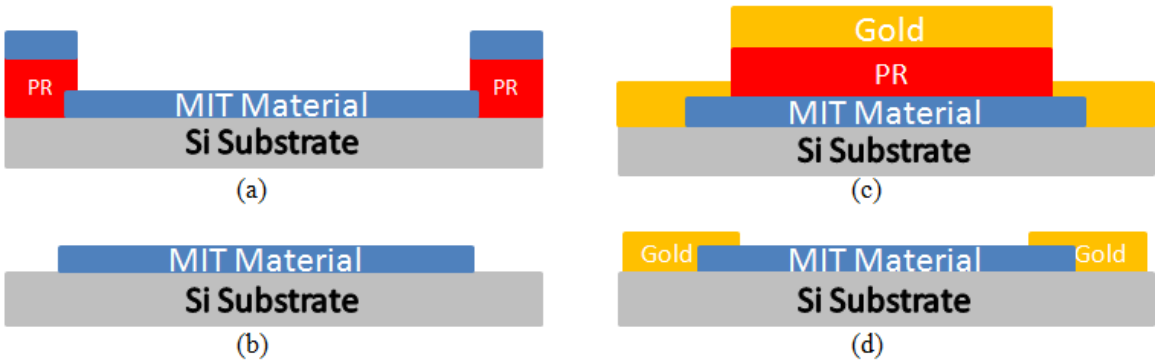

Figure 30: MIT deposition process (a) MIT sputter deposition onto Si substrate with SF-11 and 1805 photoresist, (b) after MIT liftoff and photoresist removal, (c) gold evaporated onto MIT material coated in photoresist, (d) completed DC device with gold test pads on each end of MIT wire segment.

Lift-off of the PCM was done using scotch tape followed by five minutes in an ultra sonic bath of acetone to remove any remaining material and the 1805 resist layer. The wafer is then transferred from the acetone into a beaker of 1165 remover that is heated to 90°C. After a ten minute soak, all of the SF-11 resist is removed and the 1165 remover is rinsed off with DI water and dried with nitrogen. Figure 30 (b) shows the remaining MIT wire segment on the Si substrate after the lift-off process. The step height of the PCM wires is then confirmed using the Tencor Alpha-Step IQ surface profilometer.

The PCM wires are then ready to have the test pads and parallel gold wires deposited around them. Another series of SF-11 and 1805 resists were spun onto the samples. They were then exposed to UV light through the second mask and the 1805 resist was developed. This created the windows for the test pads and parallel plate capacitor. The SF-11 was then removed from these windows by exposing the sample to a deep UV source for 200 seconds and developing it away. After removing the residual resist in the plasma asher, 50nm of titanium (Ti), deposited as an adhesion layer, and

150nm of gold (Au) were evaporated onto the samples as shown in Figure 30 (c). The Ti/Au layer was again pattered using lift-off and its thickness confirmed using the profilometer. This completed the fabrication process for all the DC devices, shown in Figure 30 (d), on the sample.

In order to deposit the ground lines for the RF device, a dielectric needed to be put on top of the parallel gold wires in order to prevent them from shorting out. SF-11 was chosen as the dielectric because it is easily patterned and is a very good electrical isolator. To pattern the SF-11, a layer of 5214 photoresist was spun on top of it. After the 5214 was post-baked, it was exposed to the third mask. Another post-bake and flood exposure followed in order to transition the resist from positive to negative. This allowed only the small dielectric areas initially exposed to the third mask to remain in the 5214 layer. A deep UV exposure was then done and the SF-11 on the rest of the sample was developed away. The remaining 5214 was finally removed using acetone, methanol, isopropyl alcohol, and DI water. This left small SF-11 blocks with sharp edge features above the parallel gold lines.

With the sharp edges of the dielectric, it would have been necessary to make the ground lines thicker than the SF-11 layer, roughly 1μm, in order to keep them from breaking as they formed a bridge over it. To avoid this, the SF-11 layer had to be reflowed in order to soften its edge features. Several different times and temperatures were tested in order to determine which resulted in the best features. In the end, the samples were baked for 90 seconds at 270°C in order to reflow the edges of the SF-11.

Since SF-11 was being used as the dielectric layer, 1818 resist was used to lift-off the ground lines. After patterning the 1818 layer with the fourth mask and developing it,

the samples were ashed to remove the residual resist. Finally, 50nm of Ti and 500nm of Au were evaporated onto the sample to form the ground lines. The excess Ti/Au was lifted-off and the 1818 removed. After one final run in the plasma asher, both the DC and RF samples were completed.

3.4 DC Electric Field Testing

Using the micromanipulator probe station shown in Figure 31, an electric field can be placed across the PCM wire using the test structures described above. During the testing, two probes are connected to an Agilent 34401A digital multimeter to measure the resistance of the PCM. A voltage is then applied to the parallel gold wires by probing the test pads at the top and bottom of the devices.

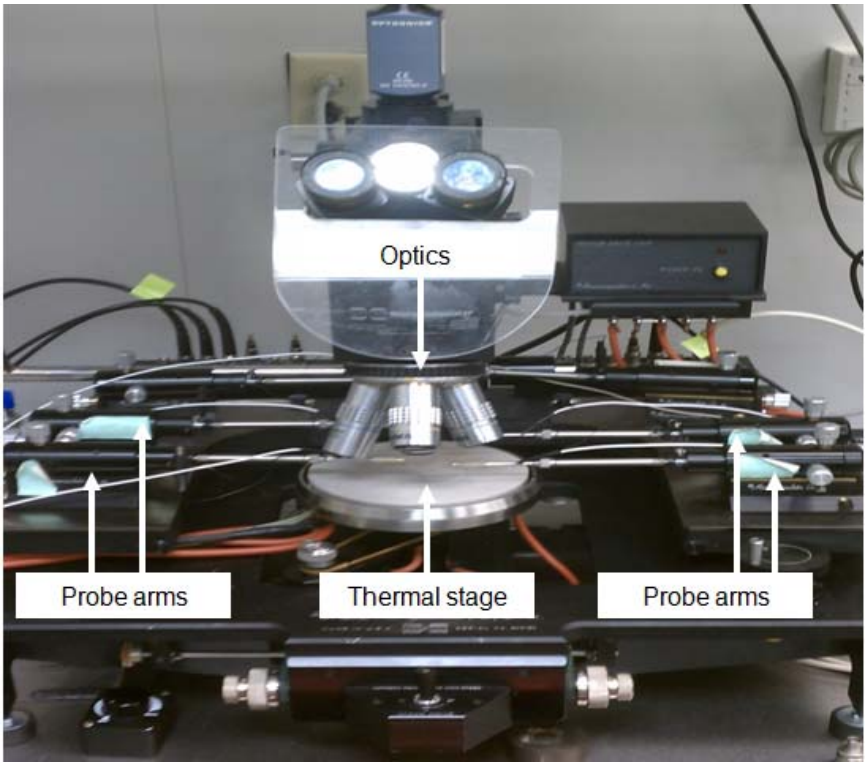

Figure 31: Micromanipulator probe station.

With the bottom plate grounded, the voltage on the top plate was varied from 0V to 200V. The parallel gold wires run nearly the entire length of the PCM in an attempt to create a phase transition across all of the material. However, it is known that fringing fields will form between the parallel lines and the PCM test pads. To counteract this effect, some devices were fabricated with shorter parallel lines. During the testing of these particular devices, it is also important to note that not all of the PCM wire may be affected by the narrower electric field.

The electric field tests were also conducted in the Lakeshore CPX cryogenic micro-manipulated probe station shown in Figure 32. The Lakeshore environmental chamber is equipped with four DC probes, two RF probes, and can be controlled from -269°C up to 202°C using liquid helium. By testing the devices in an evacuated environment, the affects of contaminants and humidity in the test room are eliminated.

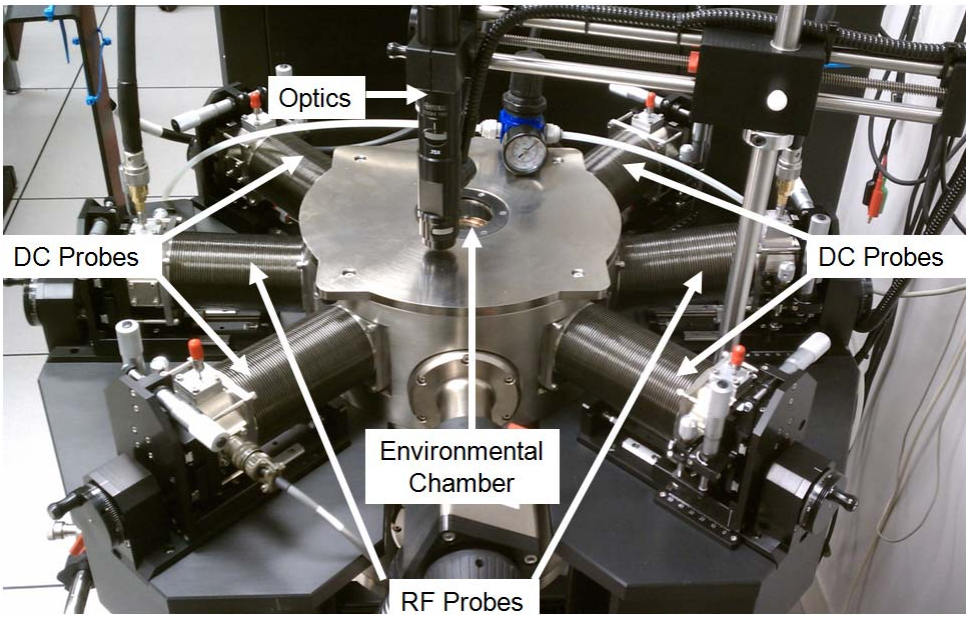

Figure 32: Lakeshore CPX cryogenic micro-manipulated probe station.

3.5 RF Device Testing

While the DC tests revolved around measuring the resistance of the PCM devices, the RF testing focused on the S parameters, the conductance or inductance, and the throughput power of the devices. The RF characteristics of PCMs were measured using ground-signal-ground and single tip probes on the RF test structures. The response of the devices was measured at frequencies from 100kHz up to 20GHz using two different methods.

First, response of the devices was measured using an Agilent 33250A arbitrary waveform generator and an Agilent E4411B spectrum analyzer. The waveform was passed through the micromanipulator probe station from one end of the PCM wire, and was received by the spectrum analyzer on the other side. While the waveforms were being passed, an electric field was applied across the PCM wires. The affect on the throughput power, in dB, was monitored from 100kHz up to 80MHz.

The RF devices were also tested using ground-signal-ground RF probes on the RF probe station, shown in Figure 33, and in the Lakeshore environmental chamber. The ground lines on the RF test structures isolate the signal line from noise, allowing a better signal to be transmitted through the device. The testing done on the Lakeshore environmental chamber used an Agilent E5070B programmable network analyzer (PNA) with a frequency range from 300kHz to 3GHz. Throughout the frequency range, an electric field was applied across the PCM wire and its response was measured. In a similar manner, the RF probe station was connected to an Agilent E8362C and tests were conducted from 10MHz up to 20GHz.

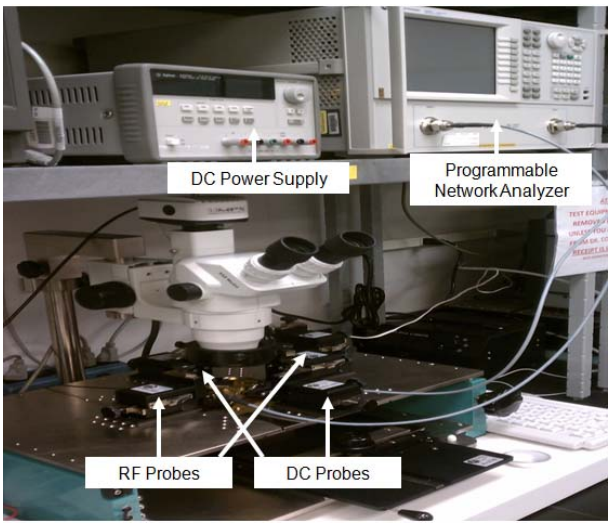

Figure 33: RF probe station connected to a programmable network analyzer (PNA).

3.6 Thermal Testing

In addition to measuring the affects of an electric field on the PCM wires, thermal affects were also measured using several heating mechanisms, each with different capabilities. In each setup, the resistance of the wires was measured by probing the test pads at the ends of the PCM. The first apparatus used to heat the PCM devices was a thermal stage monitored by an infrared camera. This stage allowed the samples to be heated from 0°C to 80°C. While this is not a very large temperature range, the exact temperature of the devices could be monitored using the IR camera as shown in Figure 34. The optics and probes connected to this thermal stage were not ideal and made testing difficult. In addition, the different emissivity of the materials on the sample also made it difficult to accurately monitor the temperature of various parts of the test structures.

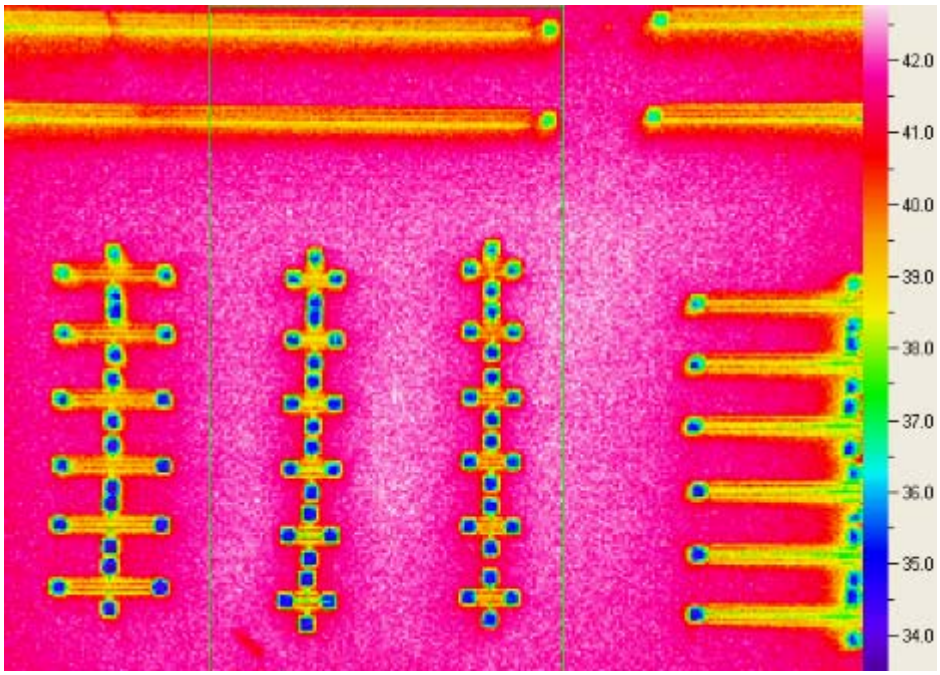

Figure 34: Thermal IR image of DC test structures (temperature scale in °C).

Thermal testing of the PCM devices was also done using the Lakeshore environmental chamber. While this stage doesn't get extremely hot, the effects of very cold temperatures on PCMs could be measured. It was also beneficial to test the devices at different temperatures in an evacuated environment. This prevented any condensation buildup on the devices, removed the affect of variations in the ambient temperature, and avoids inadvertent oxidation of the PCM wires.

Lastly, thermal testing was done using a thermal stage on the micromanipulator. This setup allowed for testing from 0°C up to 400°C. It was also the easiest to setup and control the experiments. The optics attached to this stage allowed for up to 100x zoom, making the testing of these devices much easier. While each of these heating and cooling

methods allows for a broad range of testing to be done, none of them provide the ability to rapidly heat or cool the samples.

Using the Lakeshore and micromanipulator stages, a combination of thermal and electric field stimuli were applied to the PCM devices. Each stage was elevated to its respective maximum temperature in 25°C increments. At each interval, an electric field was generated across the PCM wire by applying 0V up to 200V to the parallel capacitor. This testing shows the affect of thermal and electric field stimuli on the resistance of the PCM wires.

3.7 Alternate Heating Methods

While the thermal stages provide the ability to range the temperature of the samples from -269°C up to 400°C, they do not allow for rapid temperature change or provide the ability to heat the PCMs to their melting points. Several alternative methods were used in order to rapidly heat and cool the samples as well as methods to heat the samples to greater temperatures.

3.7.1 Meandering Heaters

In order to control the rapid heating of the samples, meandering heaters fabricated using the PolyMumps process were used. The heaters that were used for testing were designed out of polysilicon and polysilicon/gold layers, and have been heated from 80-150°C [54]. The small size of these heaters allows for localized heating and rapid cooling due to the large surface area of the substrate that will act as a heat sink.

Using the micromanipulator probe station, the heaters were carefully removed from the PolyMumps substrates and moved over to the PCM test structures. Figure 35

shows a polysilicon meandering heater placed on top of a 20µm by 600µm GeTe wire. An increasing voltage was applied across the ends of the heater while the resistance of the PCM was measured.

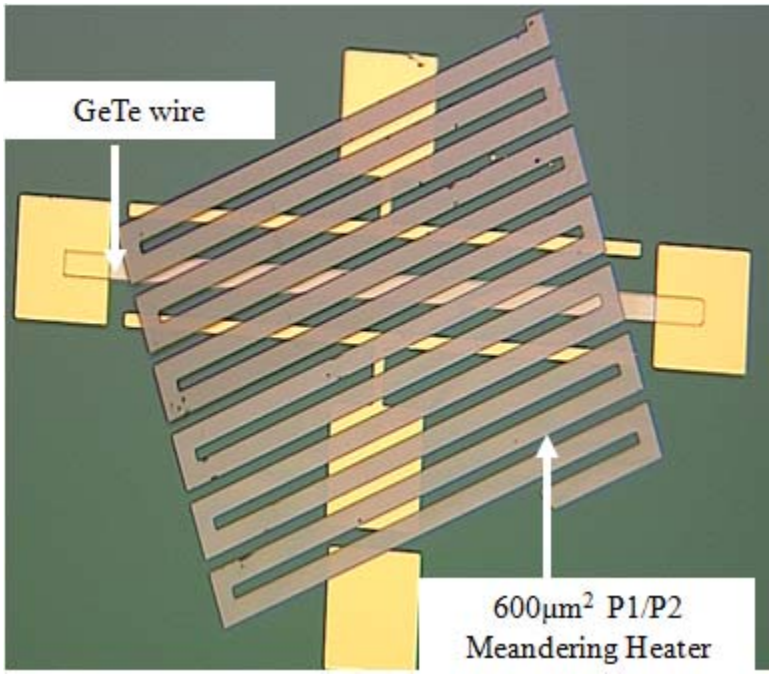

Figure 35: Polysilicon meandering heater on top of GeTe electric field test structure.

3.7.2 Thermal Flash

An alternate means of heating PCM films is to use a thermal flash system, shown in Figure 36. By concentrating a UV light through a series of lenses, a suspended sample can be heated to over 750°C while being monitored by an infrared camera. While this allows for a broad range of temperatures to be tested, the broad spot size of the beam cannot be focused on an individual test structure. Therefore, witness samples that had 200nm of the PCM layer on top of a Si_3N_4 electrical isolation layer were used. The resistivity of these samples was measured using the Jandel four point probe test bench before and after being thermally flashed.

The shutter that controls the UV light source can be opened and closed within .01 seconds, allowing for short amounts of controlled heating. Once the light source is removed, the samples will naturally cool quickly in the ambient environment. In order to accelerate the cooling process however, some samples were dropped out of the light source directly into water.

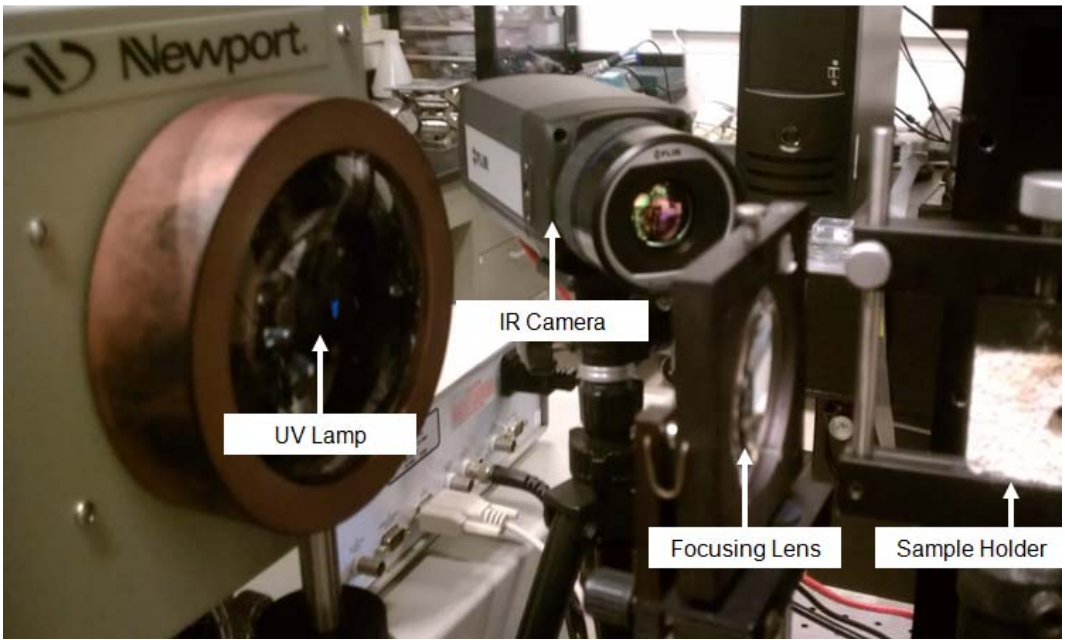

Figure 36: Thermal Flash System.

3.7.3 Joule Heating Through GeTe Wires

In order to control the localized heating of the devices to elevated temperatures, Joule heating of the PCM wires was attempted. Using the micromanipulator probe station, current was passed from one end of the PCM wire to the other, while heating the material. The waveform generator was used to apply voltage pulses from 40ns to 10ms with rise and fall times of 5ns. These short edge times allow for rapid heating and cooling of the test structures. In order to aide in heating the samples to high temperatures

and rapidly cooling them, the thermal stage on the micromanipulator was used. By elevating the stage temperature up to 350°C, while simultaneously applying current across the PCM sample, the device could reach much higher temperatures. During this experimental setup, a dry nitrogen gun was used to cool the samples more rapidly as the thermal stage returned to room temperature. In a different configuration of this setup, the thermal stage was brought down to 5°C while the current was applied. Once the current is removed, the device will cool much faster due to the lower stage temperature.

In order to determine if the duration of applied current would have an impact on the transition of the PCM wires, a constant voltage source was used. A voltage of 0-200V was applied to the ends of the PCM for 1-30 minutes. The longer the current is applied, the hotter the device will get and therefore the cooling techniques mentioned previously were employed in an attempt to quench the devices.

3.7.4 Molybdenum Heater

In order to control the localized heating to high temperatures with rapid cooling potential, a more robust heater needed to be fabricated on each individual PCM wire sample. Molybdenum (Mo) is an ideal choice for this type of heater because it has a high melting point (2623°C) and a relatively high thermal conductivity ($138 Wm^{-1}K^{-1}$). The 100nm thick Mo heater will be evaporated on top of a 50nm Ti adhesion layer and patterned using lift-off.

The heaters were designed with widths of 10, 25, 50 and 100μm in order to measure the effect of transitioning different areas of the PCM wires. An example of the 50μm heater design on top of a 200μm PCM wire is shown in Figure 37. Additionally,

two samples of each length were designed with heaters that run 75% of the length of the respective devices. These were made in an attempt to transition as much of the PCM material as possible.

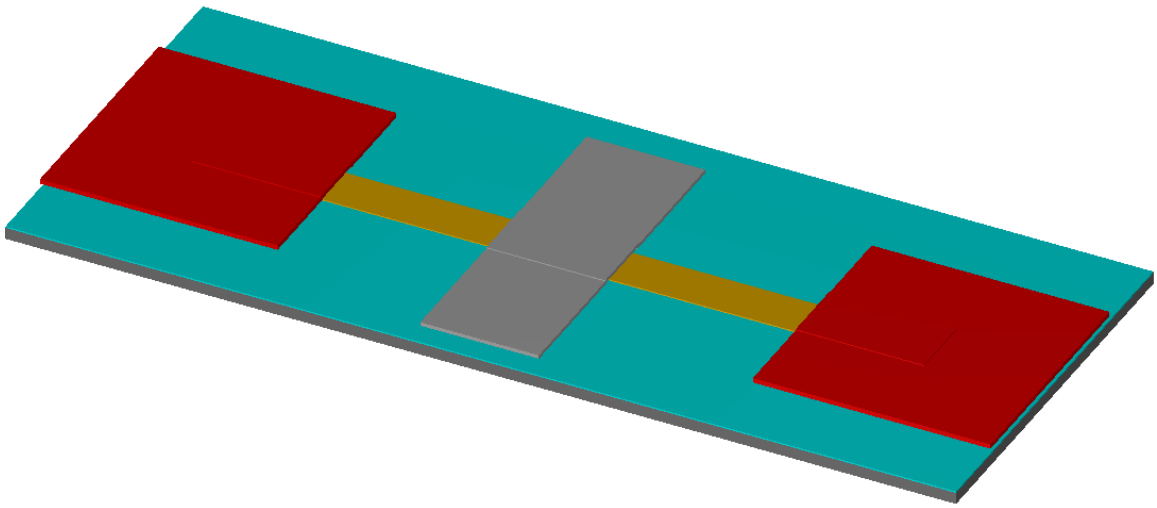

Figure 37: Thermal DC test structure with 50 µm heater.

Using the CoventorWare Finite Element Modeling (FEM) tool, the temperature of the heater could be modeled as a function of the voltage applied to the heater. The FEM image shown in Figure 38 is with 1V applied to the heater. It can be seen that the temperature is the greatest above the GeTe wire. This is caused by a large current density at this location. FEM simulations were conducted with 0-1V applied to the heater. The resulting temperatures can be seen in Table 1.

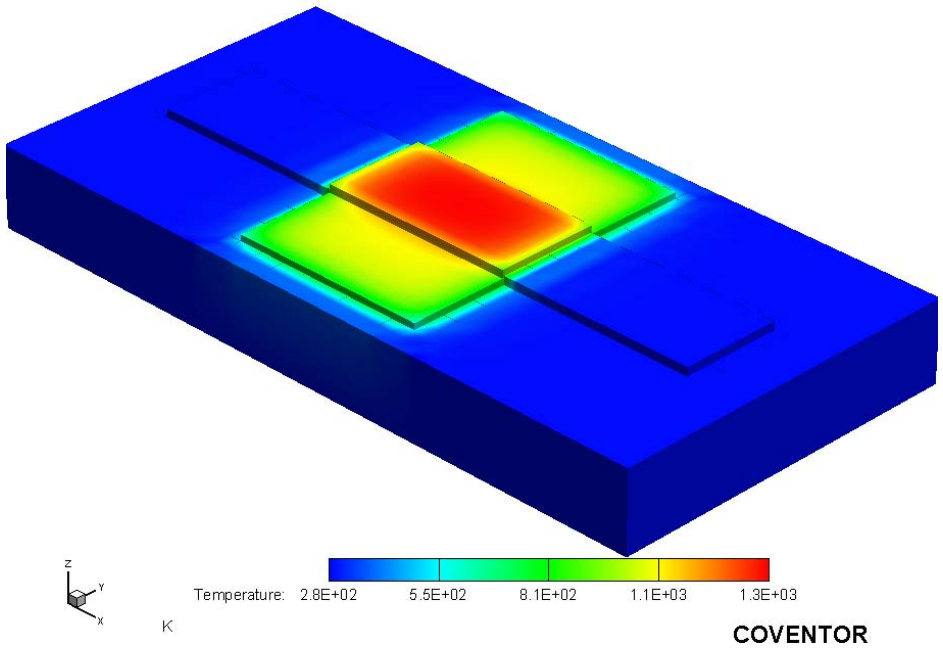

Figure 38: FEM of 200µm long PCM wire with 5V applied to the 50µm wide heater.

Table 1: Temperature as a function of the voltage applied to the 50µm wide heater.

Voltage (V)	Temperature (K)
0.0	293
.2	339
.4	468
.6	680
.8	975
1	1333

With 1V applied to the heater, the temperature on the surface of the GeTe wire directly beside the heater reached 610°C. The temperature on the very bottom of the GeTe wire increased to 1,005°C. These temperatures should be large enough to melt-quench the segment of GeTe that is under the heaters. By applying the voltage in short bursts similar

to the joule heating experiment described previously, the devices will be able to heat and cool rapidly. While the substrate will aide in removing heat from the sample, the wafer will also be placed on the thermal stage at 5°C to cool it more quickly.

3.8 Characterizing Material Properties of PCMs Amorphous and Crystalline Phases

In addition to the testing done using the micro-fabricated test structures described above, witness samples are fabricated to characterize other material properties of the PCMs. These small samples will be used to measure the resistivity, reflectivity and Young's modulus of the PCMs. The witness samples will be created in both amorphous and crystalline states so that the material properties of the two can be compared.

3.8.1 Resistivity of Deposited PCMs

In order to determine the resistivity of the PCM films, several witness samples were placed in the sputter chamber along with the sample devices. By stacking the witness samples on one another, an edge is formed as the material is sputtered. Using the profilometer, the step height of the deposited films was measured. A four point probe measurement was then done on a witness sample using the Jandel RM3-AR test unit. This provided the sheet resistance, R_s, of the film which is then multiplied by the thickness in order to find the resistivity of the sputtered PCM film.

Equation 18 was also used to determine the resistivity of the PCM films. The length and area of the structure were known by the individual device design and the profilometer measurement of the layers thickness. The resistance was then measured using the micromanipulator probe station, shown in Figure 31, by placing tungsten probe tips on the test pads at each end of the PCM wire. The probes were connected in series to

an Agilent 34401A digital multimeter. Using the device geometries and the measured resistance, the resistivity was calculated and compared to the four point probe measurements.

3.8.2 Reflectivity Measurements

When PCMs undergo a phase transition, there will be a large change in the reflectance of the material in addition to the change in resistivity. This is caused by the atomic alignment changing in the lattice structure of the sample. Using the Agilent Cary 5000 UV-Vis-NIR spectrophotometer, the reflectance of a sample can be measured at wavelengths from 175nm up to 2,200nm. This range includes near UV, visible light, and near IR wavelengths as can be seen in the electromagnetic spectrum image in Figure 39.

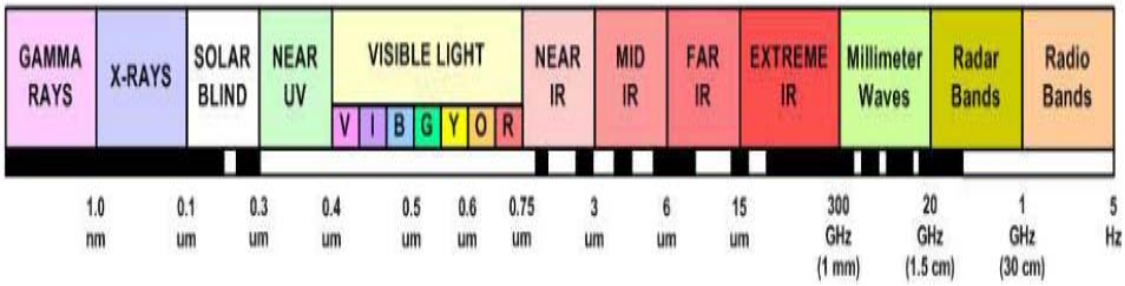

Figure 39: Wavelengths of the Electromagnetic Spectrum [59].

Due to the spot size of the Cary 5000, witness samples need to be used when measuring the reflectance of the PCM. Several GeTe samples were prepared in crystalline and amorphous phases in order to determine the difference in reflectance as well as the consistency from sample to sample. The reflectance was also measured for several different VO_x samples in order to determine the composition of the oxide.

3.8.3 Young's Modulus measurement of GeTe

As a PCM is transitioned from one phase to another, the shift in the atomic structure also causes a change in its hardness and Young's modulus. In order to measure these material properties of the GeTe films, witness samples in the crystalline and amorphous phases were used. An atomic force microscope (AFM) is used to measure the Young's modulus of the samples. The AFM will also be used to map the surface morphology of the two different samples. However, due to the small size of the AFM cantilever, it is very difficult to calibrate it to take accurate Young's modulus measurements. The AFM can still produce reliable measurements that can be used strictly for the comparison between two samples.

In order to achieve more accurate Young's modulus measurements, the nano indenter shown in Figure 40 is used. Each sample is probed in a 4x4 grid with the nano indenter tip in order to measure the average Young's modulus across the sample. As the indenter tip steps through the thickness of the material, the Young's modulus and material hardness is recorded at each nanometer step.

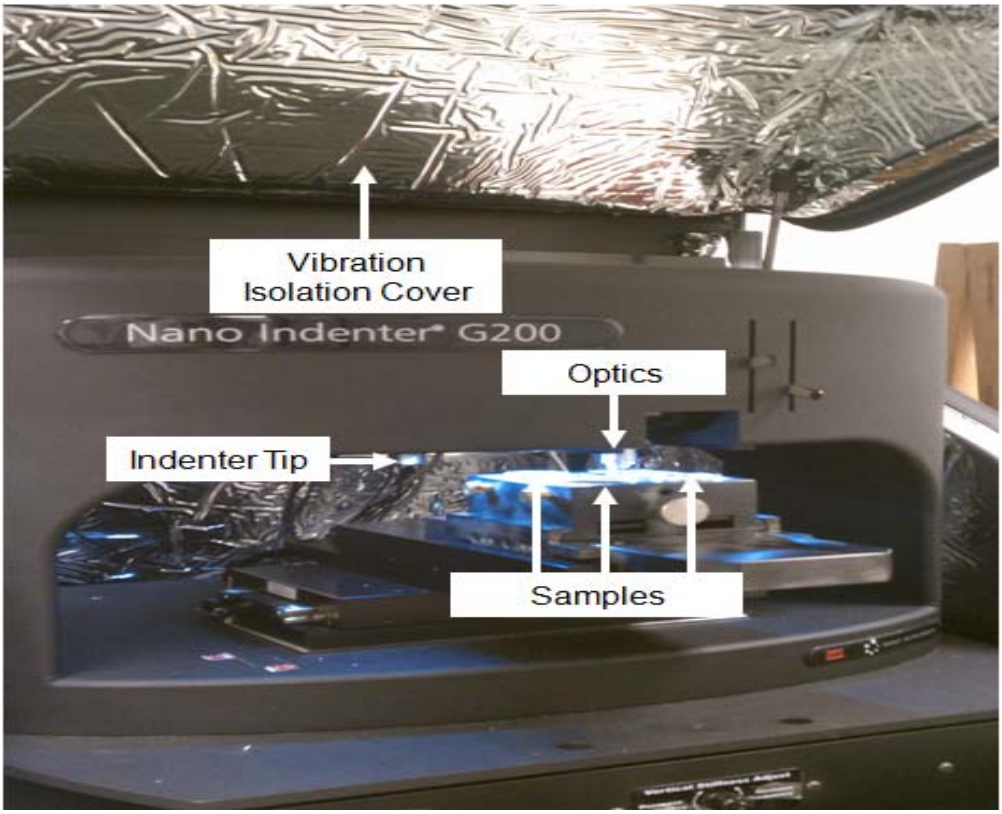

Figure 40: Nano Indenter used to measure the Young's modulus of thin films.

The average modulus recorded in the first 20nm of the witness sample film will be used as the modulus of the deposited material. This will avoid the impact of surface and substrate affects on the measurements. Once all the data is collected for the witness samples, the amorphous and crystalline results will be compared in order to determine the change in the Young's modulus that occurs during the phase transition.

3.9 Summary

This chapter described the design, fabrication, and testing of PCM test structures and witness samples. These structures provide the ability to apply thermal and electric field stimuli to the PCM wires in an attempt to generate a phase transition. The

fabrication of these devices that were laid out using the MEMS Pro L-Edit software was completed in AFIT's Class 1000 cleanroom. In order to achieve the rapid heating and cooling necessary to transition some PCM materials, a myriad of thermal tests were conducted. The results of the fabrication process and the tests described above are presented in the next chapter.

4. Results and Analysis

4.1 Chapter Overview

This chapter provides details of the test structure fabrication as well as the results of the device and witness sample testing. The analysis of the test structure design and the results of the device fabrication are presented first. Next, the results of the electric field and thermal tests are discussed. This is then followed by the measured material properties of the PCM films. Lastly, reconfigurable applications for the PCMs based on the experimental results are presented. The lessons learned from these results and the follow on work to this research are presented in the following chapter.

4.2 Test Structure Analysis

The DC and RF test structures described in the previous chapter worked well for measuring the resistance of the PCM wires. With $100\mu m^2$ test pads, probing the structures was very easy. The planar structures made it simple to apply an electric field across the PCM, but made it difficult to heat the individual devices. To counteract this setback, the molybdenum heaters were added on top of the PCM wires. By having devices of varying lengths and widths, the resistances could be compared in order to determine if the resistivity of the material was uniform across the wafer.

4.3 Results of Device Fabrication

After completing the layout and mask set for the micro test structures, the devices were successfully fabricated using VO_x and GeTe as the PCM layer. Figure 41 shows a

SEM image of an electric field test structure with a GeTe wire. On the same samples, the test structures designed for thermal testing were fabricated.

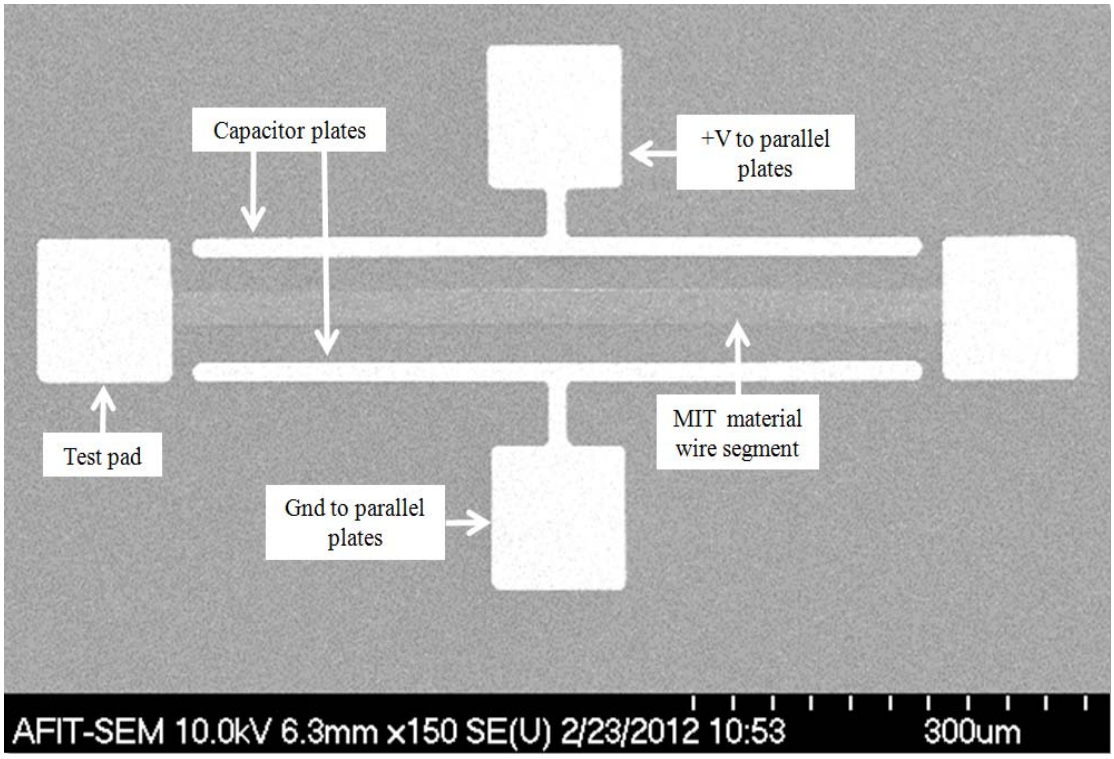

Figure 41: SEM image of electric field test structure with GeTe wire segment.

Numerous samples were created throughout this research effort, and each run produced slightly different device thicknesses. The PCM films that were sputter deposited were consistently between 190nm and 210nm thick. This was confirmed on the devices themselves and also on witness samples that were created during each PCM deposition.

The conformal nature of the PCM sputtering deposition caused small "wings" to inadvertently form during the lift-off process. Figure 42 shows these "wings" on a completed thermal test structure with a GeTe PCM wire. These wings along with slight variations in the device thickness will have an impact on the resistance of each individual

test structure. During each material deposition, witness samples were fabricated not only to confirm the thickness of the films, but also to measure their resistivity using the four point probe.

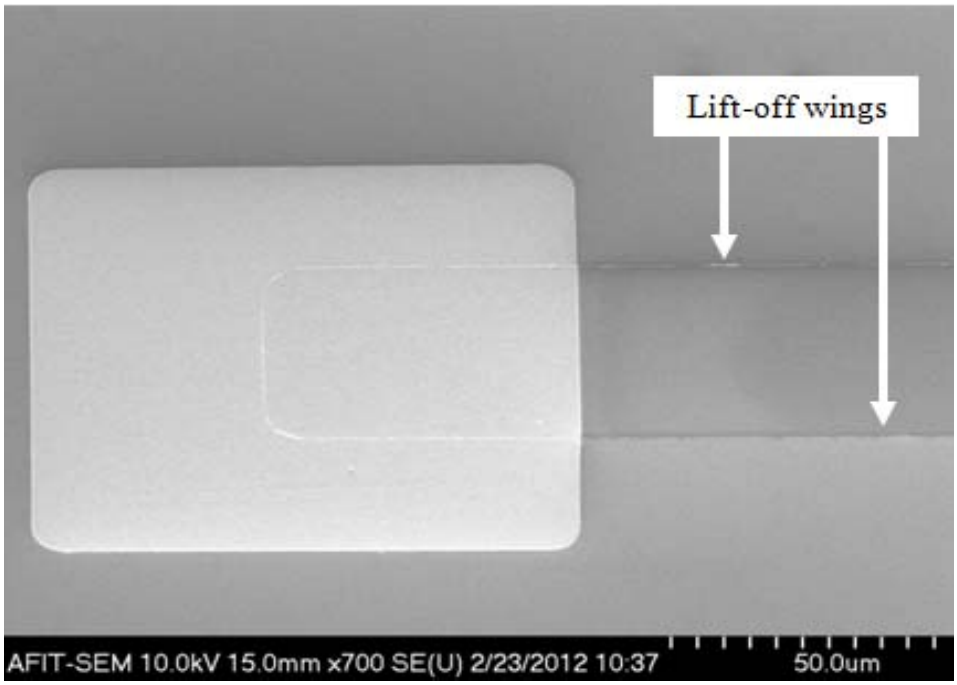

Figure 42: SEM image of thermal test structure with "wings" formed during the lift-off process.

While the GeTe devices shown in the above figures did not require any post processing, the vanadium samples needed to be oxidized after deposition in order to create the PCM. Prior to lift-off, the samples were placed in the O_2 plasma asher for 45 minutes at 150W. In order to determine the amount of oxidation that occurred in the sample, reflectivity measurements were taken and compared to known values from literature. Figure 43 shows the reflectance of the VO_x thin film. The reflectance values for the oxidized sample did not match the values for VO_2, V_2O_5, or V_6O_{13}, the most common VO_x phases, found in literature. The measurements did show a trend similar to

the fully oxidized vanadium samples. Therefore, it is concluded that the VO_x film was partially oxidized in the O_2 plasma asher, but not enough to present PCM characteristics.

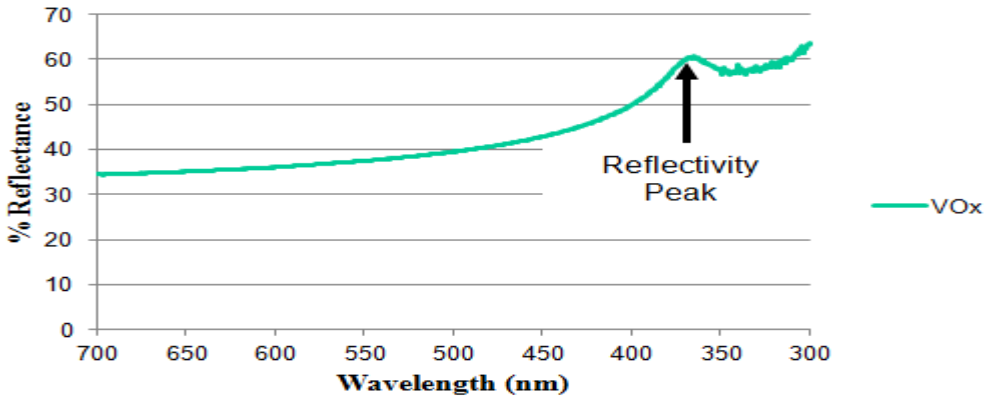

Figure 43: Reflectance of VOx thin that has been oxidized in the O_2 plasma asher.

4.4 Electric Field Testing

Initial testing was then done on the GeTe electric field test structures that were fabricated on <100> Silicon substrates. The resistance was measured across each of the GeTe wires with 0-50V applied to the parallel gold wires. Figure 44 shows the resistance across a variety of wire geometries as a varying electric field is applied.

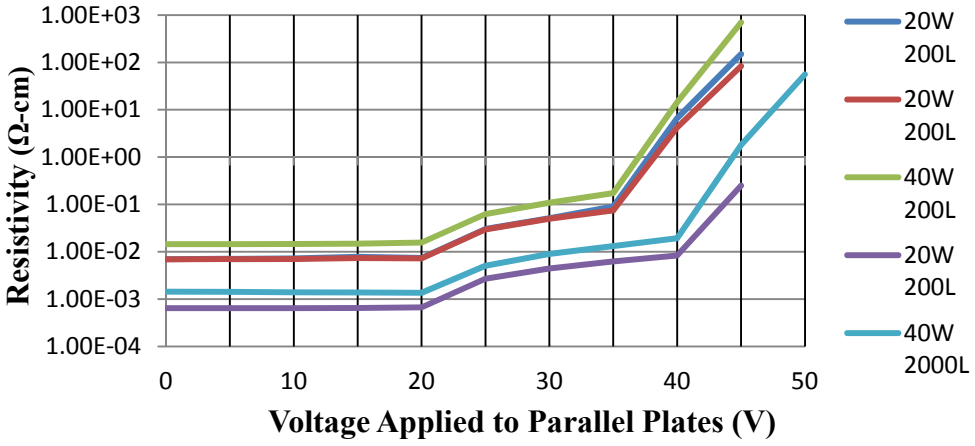

Figure 44: Resistivity of crystalline GeTe wires on <100> Silicon with the application of an electric field.

It appears that a phase transition occurs with the application of at least 40V to the parallel gold wires.

During this experiment the resistivity of the GeTe wires varied over one order of magnitude from wire to wire. This should not occur because the wires were fabricated on the same sample in order to provide uniform device characteristics. After further investigation, it was discovered that when a voltage differential was applied to the two separate parallel gold wires, a current was flowing through the substrate.

After further analysis of the test setup, it was determined that a faulty probe was being used. This probe allowed the current that was passing through the substrate to interfere with the resistance measurements that were being simultaneously taken. Therefore, it was determined that the sneak circuits that were forming through the substrate gave a false reading of a phase transition. To eliminate this problem, all further samples were prepared on a Si_3N_4 electrical isolation layer and the faulty probe was replaced.

All RF testing was done on samples that had been fabricated on wafers without the Si_3N_4 layer. The tests done with the waveform generator and spectrum analyzer resulted in an apparent small transition in the throughput power. Tests done on the RF probe station and in the Lakeshore environmental chamber showed no significant change in the throughput or reflected power as an electric field was applied across the sample. This implies that the sneak circuit created using the micromanipulator caused errant measurements on the RF test structures.

When the GeTe wires were fabricated on the Si_3N_4 layer, the resistivity of the film was consistent across the sample. Figure 45 shows the resistivity of crystalline

GeTe wire segments as an increasing electric field was applied. On the Si_3N_4 layer, no current flowed when the electric field was applied. This ensured that the resistance measurements being taken across the GeTe wires were accurate and not affected by an outside source. It can be seen in Figure 45 that as the voltage applied to the parallel gold wires is increased, there is no change in resistivity. This proves that the phase transition mechanism for GeTe films is not entirely electric field based.

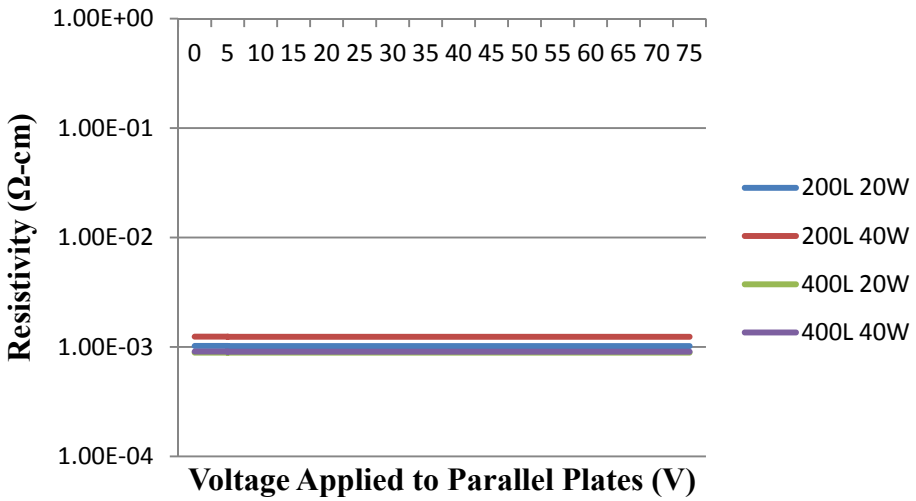

Figure 45: Resistivity of crystalline GeTe wires on Si_3N_4 electrical isolation layer with the application of an electric field.

4.5 Thermal Testing Results

Thermal testing was then done on the GeTe wire segments using three different thermal stages, one with an IR camera, one with a vacuum environment, and one with a large temperature range. The thermal stage with the IR camera was only used to monitor a crystalline sample from 23°C up to 80°C. There was no noticeable change in the sample at this temperature range.

In the Lakeshore environmental chamber, the crystalline sample was taken from room temperature up to 200°C and then from room temperature down to -269°C. It can be seen in Figure 46 (a) and (b) that there is no real change in the crystalline sample at elevated or subdued temperatures.

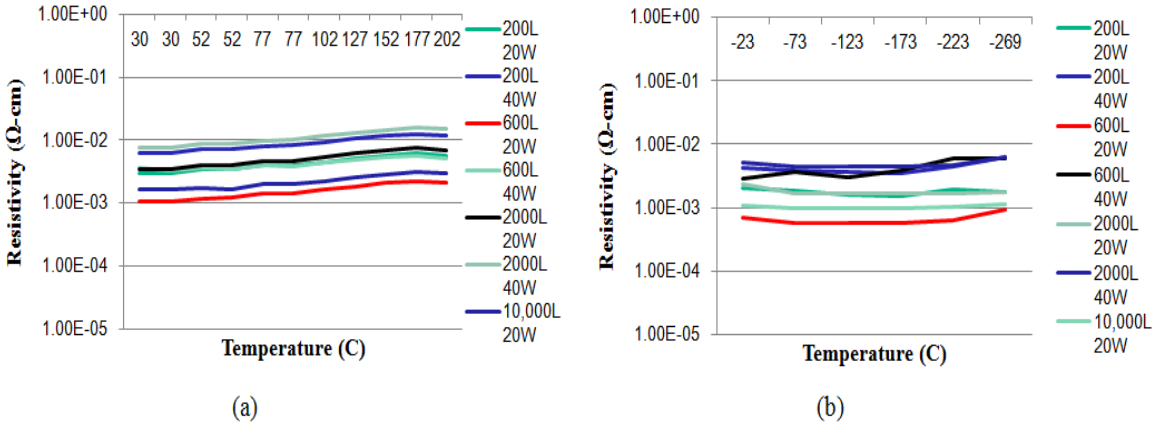

Figure 46: Resistivity of crystalline GeTe samples heated and cooled in the Lakeshore environmental chamber.

The testing done on the micromanipulator thermal stage allowed the resistance to be measured across both crystalline and amorphous GeTe wires while the samples were heated up to 400°C. Very little change was seen in the crystalline sample as the temperature was elevated, this can be seen in Figure 47.

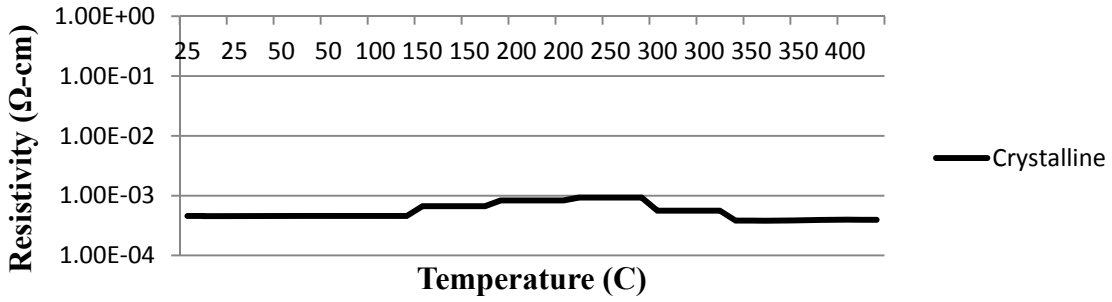

Figure 47: Resistivity of crystalline GeTe sample as temperature is increased.

As the samples were heated up to 400°C, the gold test pads began to burn up. This made taking measurements very difficult.

The resistivity of the amorphous GeTe wires, however, decreased up to two orders of magnitude as they were heated. This transition was volatile, provided they did not crystallize, and is shown in Figure 48 (b). As the samples were heated, the resistivity decreased and as soon as the samples were returned to room temperature their resistivity also returned to its initial value. Figure 48 (a) shows the samples being heated to temperatures just below 200°C. At temperatures higher than this, the samples crystallized and the transition was no longer volatile.

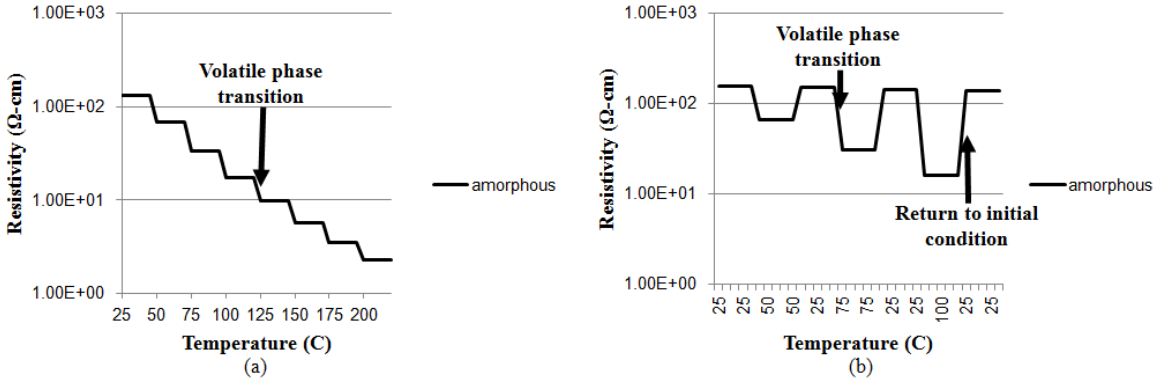

Figure 48: Resistivity of amorphous GeTe sample as it is heated and cooled.

During the volatile transition that occurs in the amorphous samples prior to crystallization, the increase in temperature causes the lattice structure to start transitioning between phases. As long as the sample is cooled prior to reaching the crystallization temperature, the particles will snap back to their original amorphous state. This two order of magnitude volatile transition, when combined with control of device geometry, can be used to design reconfigurable electrical devices.

4.6 Melt-quenching

In order to transition the crystalline GeTe wires back an amorphous state a melt-quenching mechanism needs to be used. The samples must be rapidly heated close to their melting temperature (725°C) and then quickly cooled. This will melt the crystalline GeTe into an amorphous state and rapidly freeze the lattice structure in place. Several different heating and cooling methods were attempted to melt-quench the GeTe films.

Initial testing was done on the meandering heaters to determine at what temperature they would burn out. Under the IR camera, 0- 6V were applied to a Poly1, Poly2, and Au heater. After 6V, the heater reached 125°C and then the gold trace began to burn up. A different heater was then detached from the PolyMUMPS wafer and placed on top of a 600μm long GeTe wire segment. Voltage pulses were applied to the heater after which the resistance of the GeTe wire was measured. No change in the GeTe wire resistance was seen prior to the gold trace burning up on the heater. Figure 49 (b) shows the burned out gold trace after 6V was applied. Using a Poly1, Poly2 heater, up to 68V was applied prior to the device burning up. Figure 49 (a) shows the meandering heater beginning to glow and crack as it is heated up. This too did not produce enough heat to transition the GeTe samples.

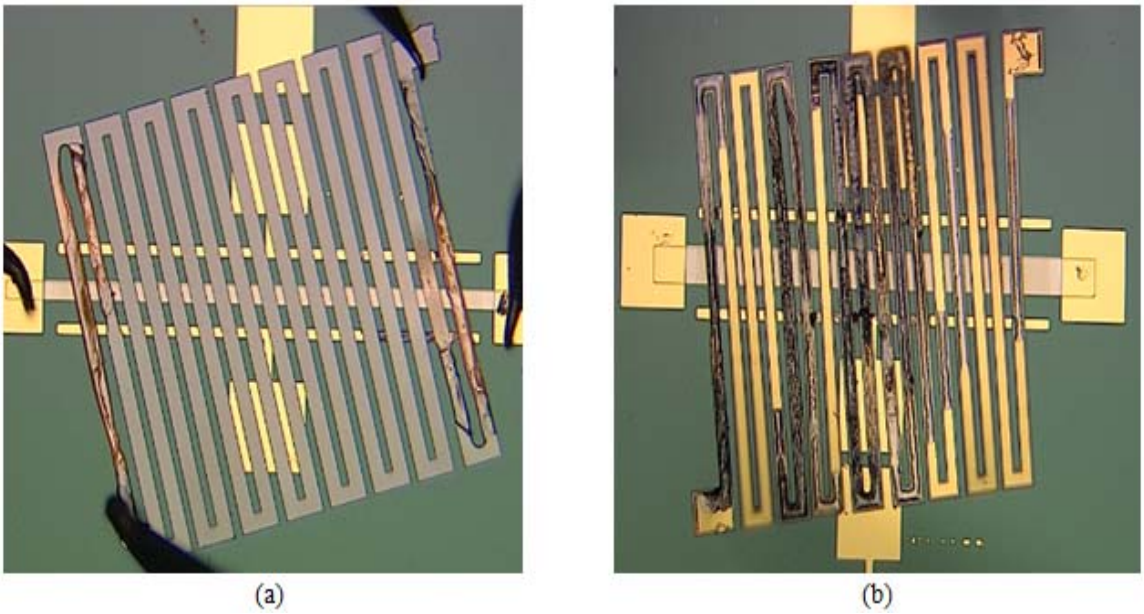

Figure 49: 600µm GeTe crystalline wire segment with (a) Poly1, Poly2 meandering heater and (b) Poly1, Poly2, Au meandering heater.

Next, the thermal flash system was used to crystallize and melt-quench the GeTe witness samples. Tests were conducted with the heat beam directed at both the GeTe surface as well as at the back of the silicon substrate that the GeTe material was sputtered onto. The amorphous samples that were heated just above their crystallization temperature showed a sudden change in temperature, as shown in Figure 50, when the phase transition occurred. Figure 50 (a) shows the temperature of the sample with the IR camera focusing on the GeTe film. The rapid loss of temperature when the sample undergoes the phase transition is not an accurate representation of the GeTe temperature. The reflectivity rapidly changes during the phase transition as shown in Figure 54 and will have a significant impact on the temperature that the IR camera reads. This is also supported by Figure 50 (b) which is focused on the backside silicon of a different amorphous GeTe sample and does not show the sudden drop in temperature. After

heating above the crystallization temperature, the shutter was closed on the thermal flash system. Once the samples were no longer being heated, they instantly began to cool. The decrease in temperature of the two samples is shown on the right sides of Figure 50 (a) and (b). After the samples reached room temperature, resistivity measurements were taken and confirmed that the amorphous samples did crystallize after being heated above 200°C.

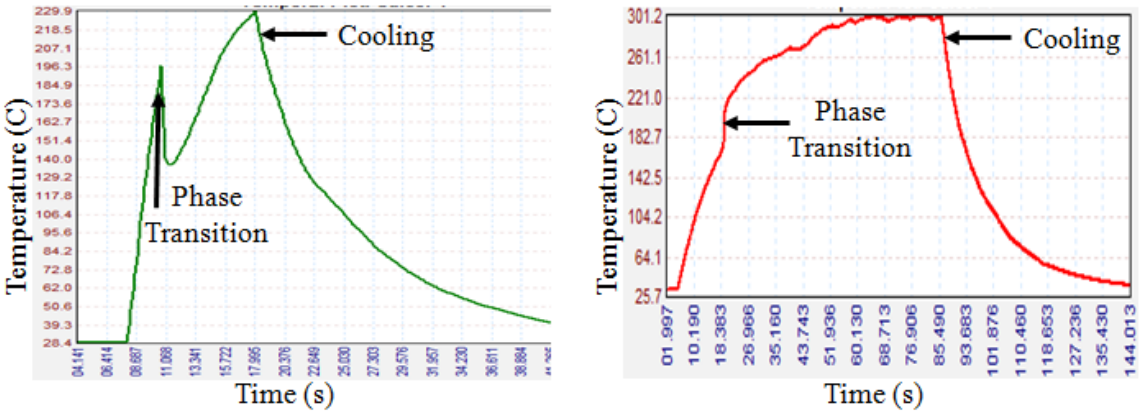

Figure 50: Thermal flash data for amorphous GeTe sample with IR camera focused on (a) GeTe film and (b) silicon substrate of GeTe film.

Crystalline samples were then heated from 250°C to 755°C. With the light source focused on the GeTe film, the samples began to burn after being heated above 450°C. At this temperature, resistivity measurements could still be taken. Once the samples were heated above this temperature, the GeTe layer began to vaporize, making resistivity measurements impossible. When the light source was directed at the substrate in order to heat the GeTe films, they were able to be heated to their melting temperature without vaporizing. Using this method, the crystalline GeTe samples were heated between 50-100% of their crystallization temperature and then cooled in the ambient environment or

dropped into a cup of water in order to rapidly cool. When cooling in air, the samples took over 15 seconds to cool back to room temperature. This is too long in order to quench the material back into an amorphous state. When cooling in water, any sample heated above 400°C underwent thermal shock due to rapid cooling and shattered. This temperature was not high enough to melt the GeTe film. It was determined that heating the large scale witness samples did not allow for rapid cooling without thermally shocking the entire sample.

In order to locally heat the small test structures, joule heating through the GeTe wire segments was also attempted. Voltage pulses from 40ns -100ms were used to try and melt-quench the crystalline GeTe samples. When the amplitude of the voltage pulses was greater than 8V, the GeTe wire would crack, as shown in Figure 51, and not allow any current to flow through the wire.

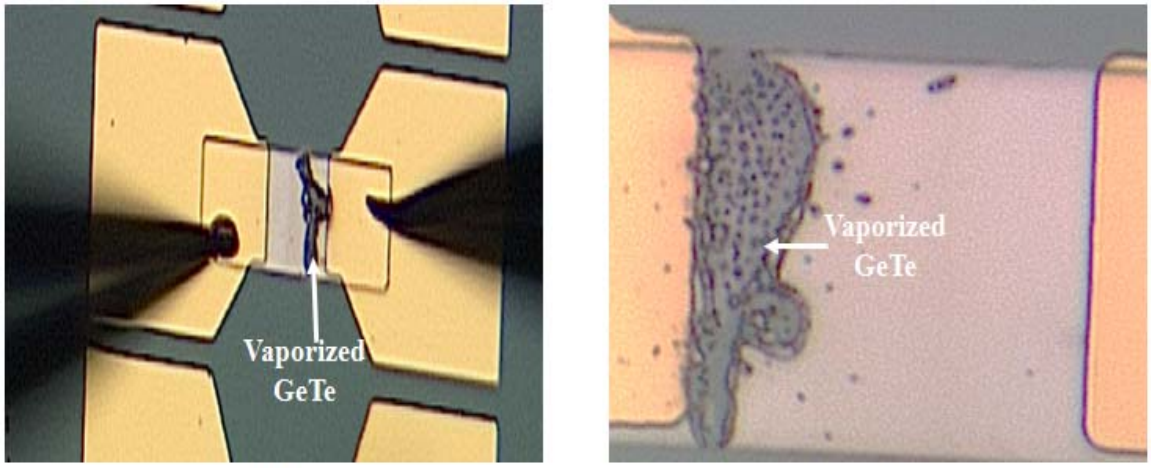

Figure 51: Crack in crystalline GeTe wire segment after 8V was applied across the wire.

Since even the small amorphous samples have extremely high resistances, it was very difficult to get any current to flow through them. Using voltage pulses, up to 220V were applied to the GeTe wire and only .02mA of current passed through. Under the assumption that even small amounts of current would eventually heat the wire up over time and possibly crystallize it, constant voltage was applied for intervals of five minutes for up to thirty minutes total. After this time, there was still no change in the resistivity of the amorphous wire segments.

Molybdenum (Mo) heaters were then deposited onto the GeTe wires to locally heat and rapidly cool them. During the evaporation process, the chamber temperature increased above the crystallization temperature and all the samples with Mo heaters became crystallized. Therefore, the heaters were used strictly to melt-quench the GeTe samples. Voltage pulses from 40ns up to 100ms were used to rapidly heat and cool the heaters. At these durations, and pulses up to 5V, there was no noticeable change in the resistivity of the GeTe wires. Once the duration of the pulses was increased past one second, the thin area of the heaters that bridged over the GeTe layer would crack. This was caused because the current density was so great in these areas that the extremely thin films could not survive the heat. In order to apply a greater voltage to the heater and not crack them at the bridge points, the probes were moved directly on top of the GeTe wire. In this position, up to 9V could be applied before the current density became too great at the 1μm probe tips and caused the Mo to burn up at those locations.

Based on the FEM modeling shown in Chapter 3 of this document, with only 1V applied to the heater, the temperature of the wire should be great enough in order for it to be melt-quenched. This is not occurring because the Mo heater is extremely conductive

and is creating an additional sneak circuit across the top of the GeTe wire. A portion of the wire may be transitioning to an amorphous state. However, when the resistance is measured from one end of the wire to the other, the current will take the path of least resistance, through the heater, and bypass the amorphous region.

4.7 Characterization of Amorphous and Crystalline GeTe Material Properties

After analyzing the results obtained from the micro-fabricated test structures, witness samples were created to characterize the material properties of amorphous and crystalline GeTe. These samples were used to measure the resistivity, reflectivity, and Young's modulus of the GeTe films.

4.7.1 Resistivity Measurements

Numerous GeTe witness samples were fabricated throughout this research effort in order to measure the resistivity of the thin films. The witness samples were prepared on a Si_3N_4 electrical isolation layer so that small leakage currents did not interfere with the measurements. Initial measurements were taken immediately after the films were sputter deposited in order to determine their state as deposited. The resistivity of the films left at room temperature was $1.4*10^3\Omega$-cm. This value is consistent with that found in literature and confirms that the GeTe films are deposited in an amorphous phase.

The phase transition for GeTe is thermally driven, so witness samples were heated to a variety of temperatures and then the resistivity was measured. The samples were heated and cooled at a rate of 10°C/min in order to avoid thermal shock. Two different sputter depositions were used to create the witness samples for this test. Figure 52 shows the resistivity of the samples after being heated to the specified temperature.

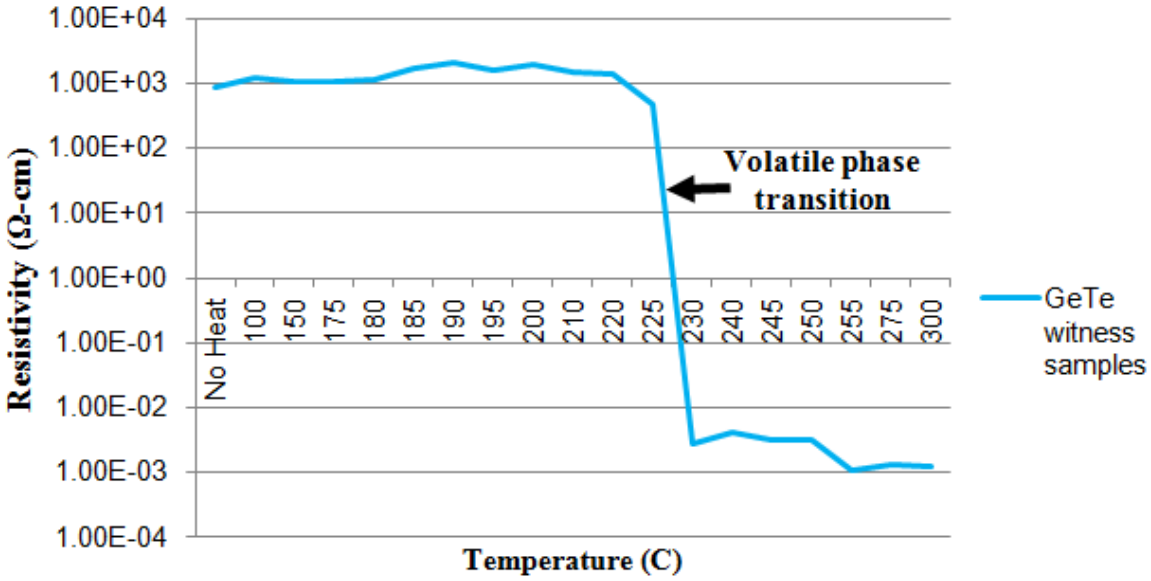

Figure 52: Resistivity measurements for GeTe thin films heated to specified temperatures at 10°C/min.

The crystallization temperature of these films was found to be approximately 230°C. This is higher than the value reported in literature, 188°C, due to the samples being heated on an open air hot plate in a laminar flow fume hood. The average resistivity of the crystallized films was $2.43*10^{-3}$Ω-cm. When the GeTe thin films crystallize, there is only a slight shift in the atoms which creates more free electrons and allows current to flow much easier. This small shift in the lattice structure is supported by the fast crystallization times reported in literature. AFM data were also collected to compare the surface morphology of the crystalline and amorphous films. Figure 53 (a) shows the particle height of an amorphous GeTe film and Figure 53 (b) shows the height of a crystalline GeTe film. The negligible difference in the surface height supports that during the crystallization process there is only a small shift in the lattice structure.

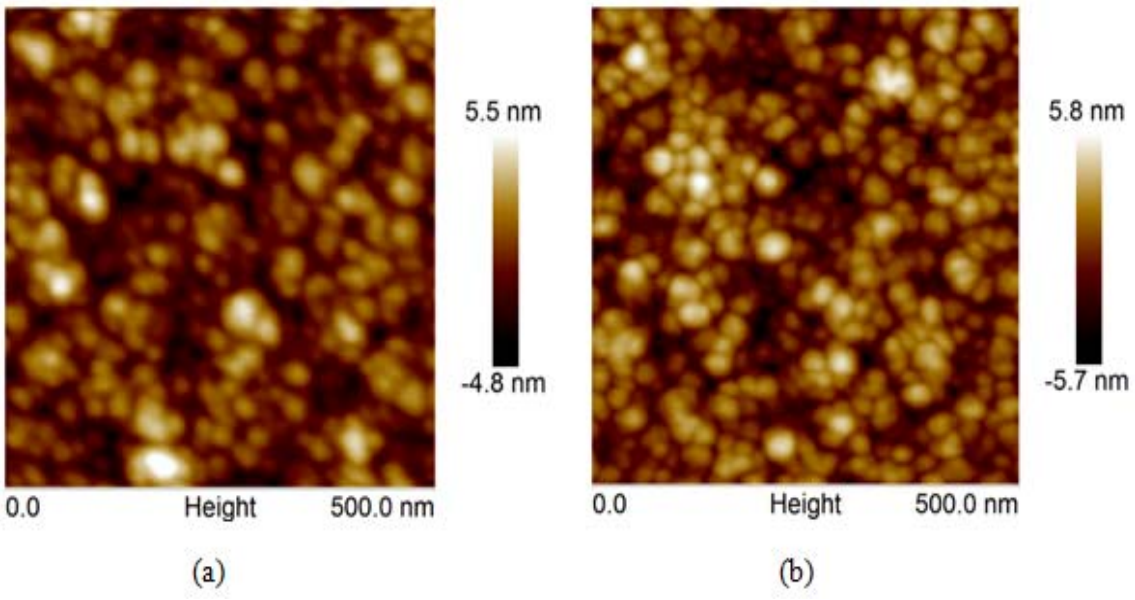

Figure 53: AFM surface morphology measurements of (a) crystalline GeTe film and (b) amorphous GeTe film.

4.7.2 GeTe Reflectivity Measurements

In addition to the resistivity measurements taken, the reflectivity of two crystalline and two amorphous samples was measured using the Cary spectrophotometer. Figure 54 shows the reflectivity for the four witness samples at wavelengths from 175nm up to 2,200nm. In the visible, 400nm – 750nm, and very low IR spectrum the reflectivity of the crystalline samples is 20-30% greater than the amorphous sample. At wavelengths greater than 900nm destructive and constructive interference patterns to occur, causing a large amount of variability in the reflectivity of both phases.

The large difference in the reflectivity is caused by a combination of reasons. The first is due to the amount of free electrons in each film. When in the crystalline state, there are many more free electrons than when the GeTe film is amorphous. This is supported by the resistivity measurements, more free electrons allow the current to flow easier, and thus the crystalline films have a lower resistivity. As the free electrons are

exposed to the incident light, they oscillate and will reflect the light. Jiles suggests that there is a direct relation between the optical reflectivity and the electrical conductivity of metals [60]. The resistivity results shown in Figure 52 and the reflectivity measurements in Figure 54 support the direct relation between higher reflectivity and higher conductivity.

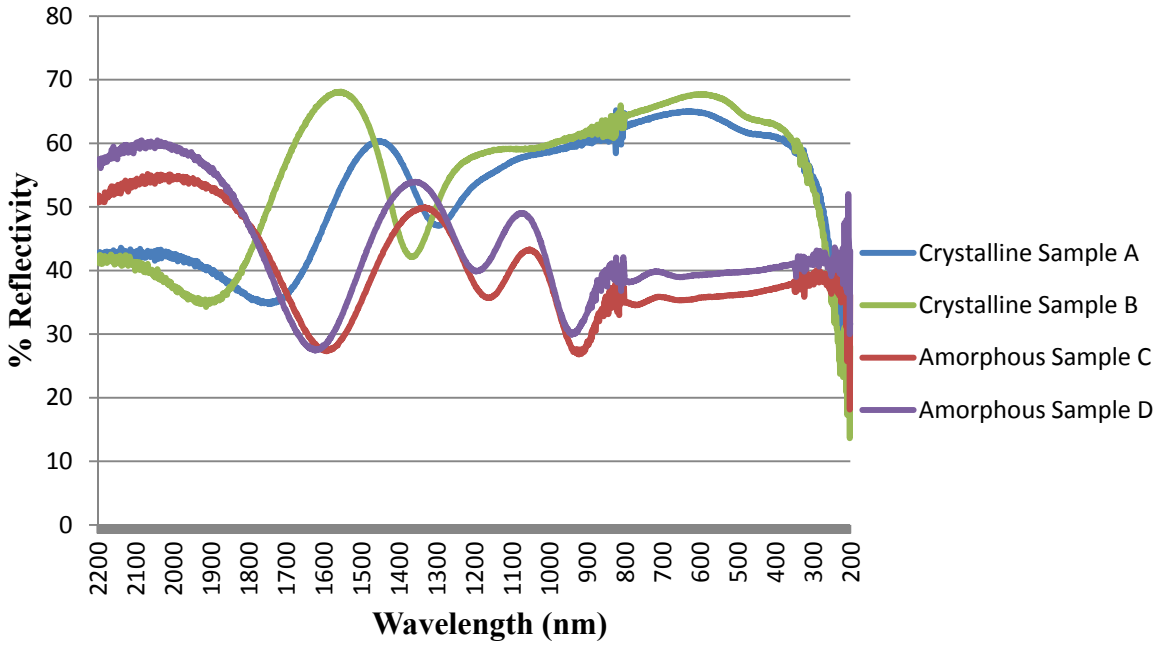

Figure 54: Reflectivity of two amorphous and two crystalline GeTe witness samples.

The second reason the crystalline films are more reflective than the amorphous films involves their surface structure. While the particle size between the two phases does not change significantly as shown in Figure 53, the atomic orientation will change when the material undergoes a transition. The non-uniformity of the amorphous films will scatter the incident light in a variety of directions. This will cause the photodetector to read a lower reflectance value. The crystalline samples, however, have a very uniform lattice structure. When the incident light hits the surface of the crystalline structure, it

will be reflected in a similar angle, creating a higher reflectance reading. The 20-30% increase in reflectance after a GeTe film is crystallized is more than enough to be taken advantage of in optical reconfigurable devices.

4.7.3 GeTe Mechanical Properties

After measuring the resistivity and reflectivity, the AFM was used to measure the Young's modulus of both amorphous and crystalline GeTe at a frequency of 2kHz. Figure 55 and Figure 56 show the resulting Young's modulus at a depth of roughly 1nm into the surface of the material. At this depth, substrate affects will not hinder the measurement.

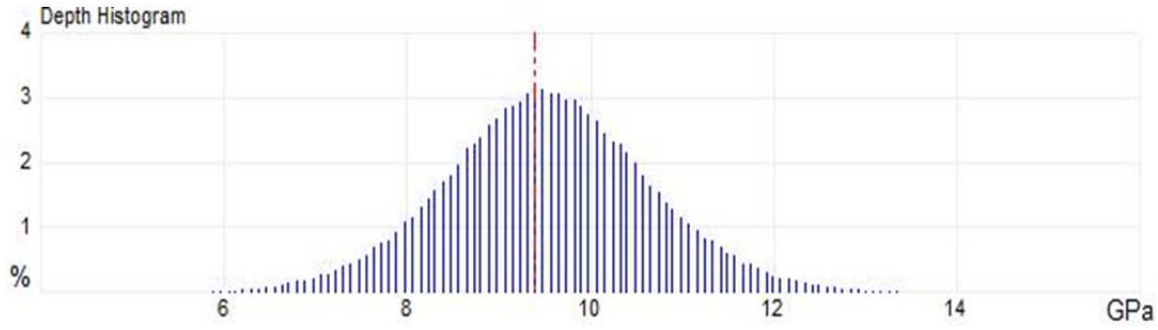

Figure 55: Young's modulus of crystalline GeTe measured using the AFM.

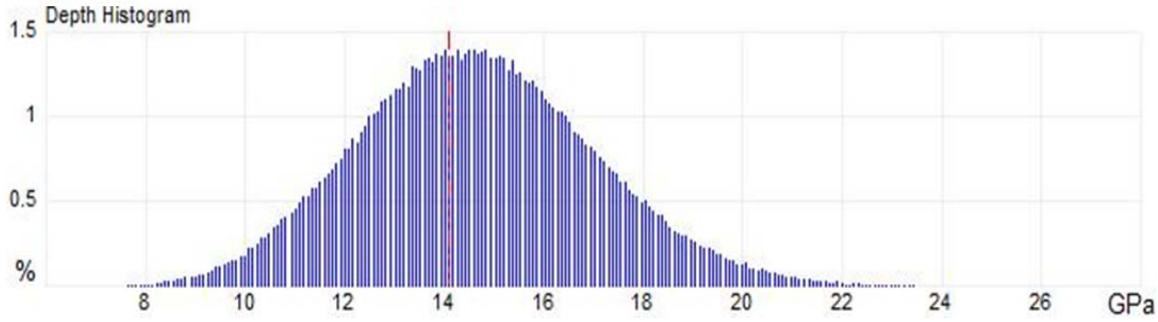

Figure 56: Young's modulus of amorphous GeTe measured using the AFM.

From Figure 56 it can be seen that the average Young's modulus measured across the surface of the amorphous GeTe sample was 14.1GPa. Figure 55 shows that the average Young's modulus for the crystalline sample was 9.3GPa. That is a 34% reduction when the GeTe samples undergo a phase transition. This is caused by the realignment of the lattice structure within the GeTe film. The uniform structure of the crystalline film will allow the particles to more easily slide past each other, making the material have a lower Young's modulus.

The AFM cantilever used to take these measurements is very small and therefore incredibly difficult to calibrate. Therefore, the absolute values of the Young's modulus found using this method are not accurate. However, the ratio between the amorphous and crystalline samples is valid because both are taken with the same AFM cantilever. A change this significant is more than enough to be taken advantage in a reconfigurable MEMS device.

A secondary test was done using a nano indenter to measure the exact Young's modulus of the samples. The initial measurement was taken at 45Hz. At this test frequency, the Young's modulus was 83.3GPa for crystalline GeTe and 62.9GPa for amorphous GeTe. That is a 28% increase when the sample is crystallized.

The contradiction of the AFM and nano indenter results is attributed to the frequency at which the measurements were taken. Since amorphous films exhibit a viscoelastic behavior, their Young's modulus measurements are frequency dependent [61]. Additional tests were completed to determine the extent of the viscoelastic effect on GeTe's Young's modulus. The Young's modulus for the amorphous sample trends downward as the frequency of the test is increased. This downward trend is caused by an

increase impact load as the modulation frequency is increased. When the impact load becomes greater than the yield stress of the material, the thin film may be showing a plastic response.

Table 2 shows the Young's modulus of an amorphous GeTe witness sample at a variety of frequencies. At frequencies higher than 300Hz, the nano indenter could not accurately collect data. This is due to the indenter tips lateral oscillation becoming greater than the threshold required to take accurate measurements.

Table 2: Young's modulus of amorphous GeTe films measured using the nano indenter at varying frequencies.

Test Frequency (Hz)	Young's Modulus (GPa)
45	62.9
100	64.1
200	38.4
300	21.3

4.8 Reconfigurable Devices

When GeTe undergoes a phase transition from amorphous to crystalline and vice versa, the resistivity, reflectivity, and Young's modulus change quite significantly as shown in Table 3. The alteration in each of these material properties during the crystallization and subsequent melt-quenching processes can be utilized in a variety of reconfigurable devices and applications. By controlling the device geometries in these components, their specific properties can be further exploited in the design and fabrication of the reconfigurable devices.

Table 3: The resistivity, reflectivity, and Young's modulus of amorphous and crystalline GeTe films

	Resistivity (Ω-cm)	Reflectivity (%)	Young's Modulus (GPa)
Amorphous	$1.4*10^{3}$	35	62.9
Crystalline	$2.43*10^{-3}$	65	83.3

As GeTe samples are crystallized, the resistivity changes six orders of magnitude from $1.4*10^{3}$Ω-cm down to $2.43*10^{-3}$Ω-cm as shown in Figure 52. Also, as shown in Figure 48, the resistivity of the amorphous samples is volatile and can be tuned from $1.4*10^{3}$Ω-cm down to $2.28*10^{0}$Ω-cm. This is a very significant change and when combined with the control of device geometries, the resistance through a reconfigurable circuit can be controlled. Figure 57 shows a variety of different wire geometries and the affect they have on the resistance of the component. Each line represents a different wire width while the thickness is fixed at 200nm and the resistivity value fixed at that of the amorphous and crystalline GeTe witness samples. Figure 57 (a) shows the resistance of crystalline GeTe wire segments while Figure 57 (b) shows the resistance of amorphous GeTe wires.

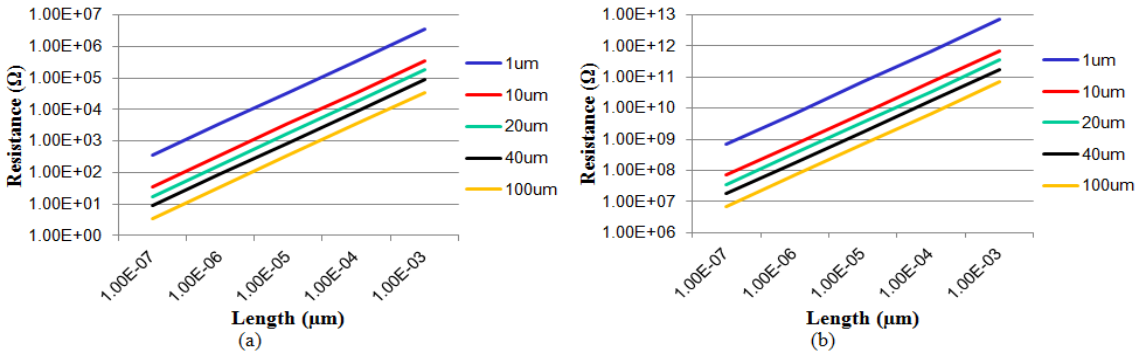

Figure 57: Resistance of (a) crystalline GeTe and (b) amorphous GeTe wire segments that are 200nm thick.

In order to take advantage of this large change in resistivity, a reconfigurable RC filter was designed. Using a circuit similar to Figure 3, a low-pass filter was designed with a GeTe wire segment in lieu of the resistor. This filter has two operating modes, mode one is a latching filter that takes advantage of the non-volatile transition and mode two utilizes the volatile transition for the filter. Using the geometries specified in Figure 57 and the resistivities measured in Figure 52, a 1μm long and 20μm wide wire segment can be created with a resistance of 607.5Ω. When this crystalline wire is placed in series with a .9pF capacitor, a low-pass filter with a cut-off frequency of 290MHz can be created. In mode one, when the wire segment undergoes a non-volatile transition to an amorphous film the cut-off frequency will be latched to 504Hz. The wire segment can then be recrystallized and the cut-off frequency will be latched to its original value. In mode two the resistivity of the GeTe wire can be tuned by heating it to a temperature just below 230°C. This tuning will allow the cut-off frequency of the filter to be varied from 504Hz to 310kHz. By simply switching the location of the resistive GeTe wire segment and the capacitor, a high-pass filter can be created with the same variable cut-off frequencies.

The change in reflectivity of the GeTe samples when they undergo a phase transition can also be utilized for reconfigurable optical devices. Using a 5mW red laser with a 670nm wavelength, a configuration can be made similar to Figure 5 that will monitor the phase transition of the GeTe sample. Based on the reflectivity measurements taken in Figure 54, the amorphous sample will reflect 35%, or 1.75mW, of power. The photodetector will recognize the crystallization of the sample as it begins to reflect 65%, or 3.25mW, of the laser power. This change will indicate that a phase transition has

occurred and also that the specific transition temperature has been reached. By adding a variety of the dopants discussed in Chapter 2, the transition temperature of GeTe can be adjusted to meet the needs of the reconfigurable temperature monitor.

An optical switching mechanism can also be created using the change in reflectivity of the GeTe samples. Using the laser described above, the photodetector can be adjusted to output an "on" signal whenever it detects a power greater than 2.5mW. This will occur when the user crystallizes the GeTe sample. When the GeTe sample is subsequently transitioned to an amorphous state, the power level will drop below the 2.5mW threshold and the photodetector will output an "off" signal. This optical switching mechanism can be employed in a variety of reconfigurable devices.

The 28% increase in the Young's modulus of GeTe when it is crystallized can be used in several reconfigurable MEMS devices. The resonant frequency of a GeTe rectangular cantilever is a function of the square root of the cantilevers Young's modulus. By controlling the geometries of the cantilever and the Young's modulus measured by the AFM (Figure 55 and Figure 56), the resonant frequency can be fluctuated from 1GHz in the amorphous phase up to 1.2GHz in the crystalline phase.

This can also be used to tune the pull-in voltage needed for an electrostatically actuated micro-switch. By specifying the geometries of the crystalline GeTe cantilever and the actuation pads, the pull-in voltage for the micro-switch will be 57.5V. When the GeTe is transitioned to an amorphous state, the pull-in voltage will drop down to 50V. This will lower the power needed to actuate the switch. If a stiffer cantilever is needed, the GeTe layer can be transitioned back to a crystalline state. In this state, the restoring

force of the cantilever will be greater and it will be more likely to overcome mechanical failure modes such as stiction.

4.9 Summary

The successful fabrication of micro test structures for PCMs was successfully completed in AFIT's class 1000 cleanroom. These devices, along with numerous witness samples, were used to characterize the transition mechanism for GeTe films. While an electric field alone cannot be used to transition the material, a thermal stimulus was successfully used to generate a phase transition. At 230°C, the amorphous as deposited films transitioned to a crystalline state. The slight alteration of the lattice structure that caused this transition affected several material properties. With additional free electrons in the crystalline state, the resistivity of the thin film decreased six orders of magnitude. This also affected the reflectivity of the GeTe film, causing it to increase 30% for wavelengths in the visible and near IR range. The Young's modulus decreased roughly 34% as well with the crystallization of the GeTe film.

The reversible transition between an amorphous state and a crystalline state can be utilized in a variety of latching reconfigurable devices. GeTe films in an amorphous state provide the ability create a volatile micro-switching mechanism that can be used in several applications. By controlling the device geometries and dopant levels, GeTe components can be configured to have material properties specific to the needs of the user. Reconfigurable circuitry, filters, optical devices, and MEMS devices can all be successfully created using a GeTe component.

5. Conclusions and Recommendations

5.1 Conclusions of Research

The need for solid state reconfigurable devices is sparked by the limited lifetime of mechanical reconfigurable components. By using a PCM device, a variety of reconfigurable mechanisms can be created. This research effort focused on characterizing the phase transitions of GeTe using micro-fabricated test structures. Additionally, reconfigurable device applications based on GeTe's phase transition and material properties were discussed. This chapter presents the main contributions produced by this research effort. Then, based on the results presented in Chapter 4, recommendations for future work are discussed. These recommendations include creating new test structures, further research and characterization of GeTe as well as other PCMs, and the design and fabrication of PCM based reconfigurable devices.

5.2 Contributions

This research effort resulted in a wide range of contributions to the characterization of PCM components for use in reconfigurable devices. These contributions will lay the ground work for future research in PCM based devices. While GeTe was the main focus of this research, the lessons learned can applied to a multitude of PCMs, further expanding the future potential of this research.

- Test structures were designed and fabricated to apply thermal and electric field stimuli to PCM wire segments
    - These structures can be used to measure the resistivity of a variety of PCMs

    - Showed that all PCM test structures need to be fabricated on an electrical isolation layer to prevent the formation of sneak circuits
- Characterized the thermal stimuli required to transition GeTe thin films from an amorphous state to a crystalline state
    - Showed that an electric field stimuli alone cannot generate a phase transition in GeTe
- Characterized the resistivity, reflectivity, and Young's modulus of both crystalline and amorphous GeTe
- Highlighted potential uses for GeTe in reconfigurable circuits, optical devices, and MEMS structures.

5.3 Future Work

There are several research avenues that can be explored based on the foundation that was established throughout this research effort. The recommendations for future work are divided into three main categories: additional characterization of GeTe, the characterization of additional PCMs, and the design and fabrication of PCM based reconfigurable devices.

5.3.1 Additional Characterizations of GeTe

When conducting further research on GeTe thin films, the focus should be on the melt-quenching process and on the RF response during the phase transition. It is well documented that melt-quenching of GeTe films requires rapid heating and cooling times as well as the ability to be generate enough heat to melt the material. Every attempt should be made to do this at the device level. This will allow for more rapid

heating/cooling as well as provide an easy transition into a real world component. Once the melt-quenching process is defined, the characterization of GeTe's RF response should be completed.

5.3.2 Additional PCM Research

An additional focus of the follow on research should be on other PCMs readily available at AFIT. Two GeSbTe compounds, VO_x, V_2O_5, and HfO_2 are just a few of the materials that can be investigated using the pre-established test structures or new test structure designs. For each of these materials, the stimulus required to generate a phase transition needs to be characterized. This may require designing and fabricating new vertical test structures. Once this stimulus has been established, work should be done to optimize the application of it as well as create a way for the stimuli to be implemented in a real world micro device. It will also be important for future research to fully characterize the material properties and RF response of each PCM in both crystalline and amorphous phases.

5.3.3 Design and Fabrication of PCM Based Reconfigurable Devices

The material properties that change during GeTe's phase transition can be utilized in a variety of reconfigurable devices, as discussed in this research. Additional reconfigurable devices should be designed to take advantage of other PCMs phase transition. Devices should also be created by combining different PCM segments in order to take full advantage of both volatile and non-volatile phase transitions. Further investigation should be done on possible PCM devices to replace traditional mechanical

micro-switching components. Lastly, follow on research should attempt to create these devices at AFIT and eventually employ them in real world military applications.

Bibliography

[1] M. Surface, "Photovoltaics: The Encyclopedia of Earth," 24 April 2010. [Online]. Available: www.eoearth.org/article/Photovoltaics. [Accessed 21 November 2012].

[2] F. Dumas-Bouchiat, C. Champeaux and A. Catherinot, "RF-Microwave Switches Based on Reversible Semiconductor-Metal Transition of VO2 Thin Films Synthesized by Pulsed Laser Deposition," *Applied Physics Letters,* vol. 91, no. 22, p. 223505, 2007.

[3] L. Perniola, V. Sousa, A. Fantini, E. Arbaoui, A. Bastard, M. Armand, A. Fargeix, C. Jahan, J. F. Nodin, A. Persico, D. Blachier, A. Toffoli, S. Loubriat, E. Gourvest, G. Betti Beneventi, H. Feldis, S. Maitrejean, S. Lhostis, A. Roule, O. Cueto, G. Reimbold, L. Poupinet, T. Billon, B. De Salvo, D. Bensahel, P. Mazoyer, R. Annunziata, P. Zuliani and F. Boulanger, "Electrical Behavior of Phase-Change Memory Cells Based on GeTe," *IEEE Electron Device Letters,* vol. 31, no. 5, pp. 488-490, 2010.

[4] S. Majumder, J. Lampen, R. Morrison and J. Maciel, "MEMS Switches," *IEEE Instrument Measurement Magazine,* vol. 6, no. 1, pp. 12-15, 2003.

[5] M. Braunovic, V. Konchits and N. Myshkin, Electrical Contacts - Fundamentals, Applications, and Technology, New York: CRC Press, 2007.

[6] G. Rabeiz, RF MEMS, theory, design, and technology, Hoboken: John Wiley and Sons, 2004.

[7] Z. Yang, D. Lichtenwalner, A. Morris, J. Krim and A. Kingon, "Comparison of Au and Au-Ni Alloys as Contact Materials for MEMS Switches," *IEEE Journal of Microelectromechanical Systems,* vol. 18, no. 2, pp. 287-295, 2009.

[8] R. R. Ludeman, Introduction to Electronic Devices and Circuits, Orlando: Holt, Rinehart, and Winston, Inc., 1990.

[9] S. J., Y. Wang and I. T., "Reconfigurable quasi-fractal transmission line structures," in *IEEE International Microwave Symposium*, Seattle, 2002.

[10] D. Peroulis, S. Pacheco, K. Sarabandi and L. Katehi, "Tunable lumped components with applications to reconfigurable MEMS filters," in *IEEE International Microwave Symposium*, Phoenix, 2001.

[11] S. Lee, J.-H. Park, J.-M. Kim, H.-T. Kim, Y.-K. Kim and Y. Kwon, "A compact low-loss reconfigurable monolithic low-pass filter using multiple-contact MEMS switches," *IEEE Microwave and Wireless Components Letters,* vol. 14, no. 1, pp. 37-39, 2004.

[12] L. Ke, *A Method of Light Reflectance Measurement,* The University of British Columbia, 1999.

[13] E. Hecht, Optics, San Francisco: Pearson Education, Inc., 2002.

[14] S. Raoux, H. Y. Cheng and H. S. P. Wong, "Crystallization times of Ge-Te phase change materials as a function of composition," *Applied Physics Letters,* vol. 95, no. 7, p. 071910, 2009.

[15] M. E. Motamedi, MOEMS Micro-Opto_Electro-Mechanical Systems, Bellingham: SPIE- The International Society of Optical Engineering, 2005.

[16] A. Torii, M. Sasaki, K. Hane and S. Okuma, "A method for determining the spring constant of cantilevers for atomic force microscopy," *Measurement Science and Technology,* vol. 7, no. 2, p. 179, 1996.

[17] S. Chakraborty and T. Bhattacharyya, "Development of a surface micro-machined binary logic inverter for ultra-low frequency MEMS sensor applications," *Journal of Micromechanics and Microengineering,* vol. 20, no. 10, p. 105026, 2010.

[18] H. Jaafar, "Design and simulation of high performance RF MEMS series switch," in *IEEE Regional Symposium on Micro and Nanoelectronics (RSM)*, Serdang, Malaysia, 2011.

[19] K. Van Caekenberghe, "RF MEMS on the radar," *IEEE Microwave Magazine,* vol. 10, no. 6, pp. 99-116, 2009.

[20] S. Majumder, N. McGruer, G. Adams, P. Zavracky, R. Morrison and J. Krim, "Study of contacts in an electrostatically actuated microswitch," *Sensors Actuators,* vol.

93, no. 1, pp. 19-26, 2001.

[21] E. K. Chua, L. P. Shi, R. Zhao, K. G. Lim, T. C. Chong, T. E. Schlesinger and J. A. Bain, "Low resistance, high dynamic range reconfigurable phase change switch for radio frequency applications," *Applied Physics Letters,* vol. 97, no. 18, p. 183506, 2010.

[22] M. Di Ventra and Y. V. Pershin, "Memory Materials: A Unifying Description," *Materials Today,* vol. 14, no. 12, pp. 584-591, 2011.

[23] A. Bastard, J. C. Bastien, B. Hyot, S. Lhostis, F. Mompiou, C. Bonafos, G. Servanton, C. Borowiak, F. Lorut, N. Bicais-Lepinay and A. Toffol, "Crystallization Study of Melt Quenched Amorphous GeTe by Transmission Electron Microscopy for Phase Change Memory Applications," *Applied Physics Letter,* vol. 99, no. 24, p. 3103, 2011.

[24] M. Chen, K. A. Rubin and R. W. Barton, "Compound Materials for Reversible, Phase-Change Optical Data Storage," *Applied Physics Letters,* vol. 49, p. 502, 1986.

[25] J. H. Coombs, A. P. J. M. Jongenelis, W. Van Es-Spiekman and B. A. J. Jacobs, "Laser-induced crystallization phenomena in GeTe-Based Alloys. I. Characterization of nucleation and growth," *Journal of Applied Physics,* vol. 78, no. 8, p. 4906, 1995.

[26] G. Bruns, P. Merkelbach, C. Schlockermann, M. Salinga, M. Wuttig, T. D. Happ, J. B. Philipp and M. Kund, "Nanosecond Switching in GeTe Phase Change Memory Cells," *Applied Physics Letters,* vol. 95, p. 043108, 2009.

[27] A. N. S. Institute, *American National Standard for Safe Use of Lasers: ANSI Z136.1,* 2007.

[28] J. Kalb, F. Spaepen and M. Wuttig, "Atomic Force Microscopy Measurement of Crystal Nucleation and Growth Rates in Thin Films of Amorphous Te Alloys," *Applied Physics Letters,* vol. 84, no. 25, pp. 5240-5242, 2004.

[29] K.-H. Song, S.-C. Beak and H.-Y. Lee, "Amorphous-to-crystalline phase transition of (InTe)x(GeTe) thin films," *Journal of Applied Physics,* vol. 108, no. 2, p. 024506, 2010.

[30] N. Pashkov, G. Navarro, J. C. Bastien, M. Suri, L. Perniola, V. Sousa, S. Maitrejean, A. Persico, A. Roule, A. Toffoli, G. Reimbold, B. De Salvo, O. Faynot, P. Zuliani and R. Annunziata, "Physical and Electrical Characterization of Germanium or Tellurium rich GexTe1-x for Phase Change Memories," in *Solid-State Device Research Conference*, Helsinki, Finlad, 2011.

[31] S. Lai and T. Lowrey, "OUM - A 180 nm Nonvolatile Memory Cell Element Technology For Stand Alone and Embedded Applications," in *Electron Devices Meeting*, Washington D.C., 2001.

[32] J. H. Coombs, A. P. J. M. Jongenelis, W. Van Es-Spiekman and B. A. J. Jacobs, "Laser-Induced Crystallization Phenomena in GeTe-based alloys. II. Composition Dependence of Nucleation and Growth," *Journal of Applied Physics,* vol. 78, no. 8, p. 4918, 1995.

[33] D. Lelmini and A. L. Lacaita, "Phase Change Materials In Non-Volatile Storage," *Materials Today,* vol. 14, no. 12, pp. 600-607, 2011.

[34] S.-J. Choi, K.-H. Kim, G.-S. Park, H.-J. Bae, W.-Y. Yang and S. Cho, "Multibit Operation of Cu/Cu-GeTe/W Resistive Memory Device Controlled by Pulse Voltage Magnitude and Width," *Electron Device Letter, IEEE,* vol. 32, no. 3, pp. 375-377, 2011.

[35] Y. Sutou, T. Kamada, Y. Saito, M. Sumiya and J. Koike, "Phase Change Behavior of Ge1Cu2Te3 Films," in *European Phase Change and Ovonics Science Symposium*, Zurich, Switzerland, 2011.

[36] J.-J. Lee, S.-G. Yoon, K.-J. Choi, S.-O. Ryu, S.-M. Yoon, N.-Y. Lee and B.-G. Yu, "Characterization of in situ diffusion of silver in Ge-Te amorphous films for programmable metallization cell memory application," *Journal of Vacuum Science and Technology B: Microelectronics and Nanometer Structures,* vol. 24, no. 5, pp. 2312-2316, 2006.

[37] A. Fantini, L. Perniola, M. Armand, J. F. Nodin, V. Sousa, A. Persico, J. Gluzel, C. Jahan, S. Maitrejean, S. Lhostis, A. Roule, C. Dressler, G. Reimbold, B. De Salvo, P. Mazoyer, D. Bensahel and F. Boulanger, "Comparative Assessment of GST and GeTe Materials for Application to Embedded Phase-Change Memory Devices," in *IEEE International Memory Workshop*, Monterey, 2009.

[38] Y. Lu, S. Song, Z. Song, L. Wu, B. Liu, S. Feng and X. Guo, "Study on TiO2-doped Ge2Te3 films for phase-change memory application," *Journal of Physics D: Applied Physics,* vol. 44, no. 14, p. 145102, 2011.

[39] S.-J. Yang, J.-M. Lee, K. Shin, H.-Y. Lee and H.-B. Chung, "Electrical switching studies of se-doped germanium telluride glasses," in *Microprocesses and Nanotechnology Conference*, Osaka, Japan, 2004.

[40] A. Devasia, S. Kurinec, K. Campbell and S. Raoux, "Influence of Sn Migration on phase transition in GeTe and Ge2Se3 thin films," *Applied Physics Letters,* vol. 96, no. 14, p. 141908, 2010.

[41] J.-S. Choi, H.-J. Kim, H.-C. Kim, T.-S. Oh, D.-B. Hyun and H. Lee, "Thermoelectric properties of n-type (Pb1-xGex)Te fabricated by hot pressing method," in *international Conference on Thermoelectrics*, Dresden, Germany, 1997.

[42] Y. Fukuma, M. Arifuku, H. Asada and T. Koyanagi, "Growth of ferromagnetic semiconductor Ge1-xMnxTe films on BaF2 (111) by ionized cluster beam deposition," *Journal of Applied Physics,* vol. 97, no. 7, p. 073910, 2005.

[43] Y. Liu, S. K. Bose and J. Kudrnovsky, "Half-metallicity and magnetism of GeTe doped with transition metals V, Cr, and Mn: A theoretical study from the viewpoint of application in spintronics," *Journal of Applied Physics,* vol. 112, no. 5, p. 053902, 2012.

[44] Y. Fukuma, H. Asada, J. Miyashita, N. Nishimura and T. Koyanagi, "Magnetic properties of IV-VI compound GeTe based diluted magnetic semiconductors," *Journal of Applied Physics,* vol. 93, no. 10, pp. 7667-7669, 2003.

[45] A. Pirovano, F. Pellizzer, I. Tortorelli, A. Rigano, R. Harrigan, M. Magistretti, P. Petruzza, E. Varesi, A. Redaelli, D. Erbetta, T. Marangon, F. Bedeschi, R. Fackenthal, G. Atwood and R. Bez, "Phase-Change Memory Technology With Self-Aligned uTrench Cell Architecture for 90 nm Node and Beyond," *Solid-State Electronics,* vol. 52, no. 9, pp. 1467-1472, 2008.

[46] A. Z. Moshfegh and A. Ignatiev, "Formation and Characterization of Thin Film Vanadium Oxides: Auger Electron Spectroscopy, X-Ray Photoelectron Spectroscopy, X-Ray Diffraction, Scanning Electron Microscopy, and Optical Reflectance Studies," *Thin Solid Films,* vol. 198, no. 1-2, pp. 251-268, 1991.

[47] S. Surnev, M. G. Ramsey and F. P. Netzer, "Vanadium Oxide Surface Studies," *Progress in Surface Science,* vol. 73, no. 4-8, pp. 117-165, 2003.

[48] F. Cilento, C. Giannetti, G. Ferrini, S. Dal Conte, T. Sala, G. Coslovich, M. Rini, A. Cavalleri and F. Parmigiani, "Ultrafast insulator-to-metal phase transition as a switch to measure the spectrogram of a supercontinuum light pulse," *Applied Physics Letters,* vol. 96, no. 2, p. 021102, 2010.

[49] A. Pergament, "Metal-Insulator Transition: The Mott Criterion and Coherence Length," *Journal of Physics: Condensed Matter,* vol. 15, no. 19, p. 3217, 2003.

[50] T.-R. Shen, T.-K. Yang, L. Ming-Hong, F. I-Ping, L. Nai-Yun and W.-T. Chen, "Synthesis and characterization of vanadium oxides by hydrothermal method for hydrogen production under visible light," in *Internation Converence on Chemistry and Chemical Engineering*, Kyoto, Japan, 2010.

[51] J. Givernaud, C. Champeaux, A. Catherinot, A. Pothier, P. Blondy and A. Crunteanu, "Tunable Band Stop Filters based on Metal-Insulator Transition in Vanadium Dioxide Thin Films," in *IEEE International Microwave Symposium Digest*, Atlanta, 2008.

[52] D. Bouyge, A. Crunteanu, J. C. Orlianges, D. Passerieux, C. Cahmpeaux, A. Catherinot, A. Velez, J. Bonache, F. Martin and P. Blondy, "Reconfigurable Bandpass Filter Based on Split Ring Resonators and Vanadium Dioxide (VO2) Microwave switches," in *Asia Pacific Microwave conference*, Singapore, 2009.

[53] L. A. L. de Almeida, G. S. Deep, A. M. N. Lima, I. A. Khrebtov, V. G. Malyarov and H. Neff, "Modeling and Performance of Vanadium-Oxide Transtion Edge Microbolometers," *Applied Physics Letters,* vol. 85, no. 16, p. 3605, 2004.

[54] S. Ostrow, *Microelectromechanical systems (MEMS) Designs For Anti-Tamper Response Applications,* Wright-Patterson AFB OH: Air Force Institute of Technology (AU), 2011.

[55] J. Carter, A. Cowen, B. Hardy, R. Mahadevan, M. Stonefield and S. Wilcenski, *PolyMUMPs design handbook revision 11.0.*

[56] S. Franssila, Introduction to Microfabrication, West Sussex, United Kingdom: John Wiley & Sons, Ltd, 2010.

[57] R. W. Johnstone, *Automated desin for micromachining: Resistor, snake,* 2006.

[58] F. A. Chudnovskii, L. L. Odynets, A. L. Pergament and G. B. Stefanovich, "Electroforming and Switching in Oxides of Transition Metals: The Role of Metal-Insulator Transition in the Switching Mechanism," *Journal of Solid State Chemistry,* vol. 122, no. 1, pp. 95-99, 1996.

[59] E. Williams, C. maraviglia and A. Moran, "From X-rays to radar: using color to understand imagery," in *Applied Imagery Pattern Recognition Workshop*, Washington DC, 2002.

[60] D. Jiles, Introduction to the Electronic Properties of Materials, United Kingdom: Nelson Thornes Ltd, 2001.

[61] M. A. Meyers and K. K. Chawla, Mechanical Behavior of Materials, Upper Saddle River: Prentice-Hall, Inc., 1999.

REPORT DOCUMENTATION PAGE

Form Approved
OMB No. 074-0188

1. REPORT DATE *(DD-MM-YYYY)*	2. REPORT TYPE	3. DATES COVERED *(From – To)*
21-03-2013	Master's Thesis	Aug 2011 – Mar 2013

4. TITLE AND SUBTITLE
Characterization of Metal-Insulator-Transition (MIT) Phase Change Materials (PCM) for Reconfigurable Components, Circuits, and Systems

5a. CONTRACT NUMBER

5b. GRANT NUMBER

5c. PROGRAM ELEMENT NUMBER

6. AUTHOR(S)
Danner, Brent L., 2LT, USAF

5d. PROJECT NUMBER
N/A

5e. TASK NUMBER

5f. WORK UNIT NUMBER

7. PERFORMING ORGANIZATION NAMES(S) AND ADDRESS(S)
Air Force Institute of Technology
Graduate School of Engineering and Management (AFIT/EN)
2950 Hobson Way, Building 640
WPAFB OH 45433

8. PERFORMING ORGANIZATION REPORT NUMBER
AFIT-ENG-13-M-12

9. SPONSORING/MONITORING AGENCY NAME(S) AND ADDRESS(ES)
Intentionally Left Blank

10. SPONSOR/MONITOR'S ACRONYM(S)

11. SPONSOR/MONITOR'S REPORT NUMBER(S)

12. DISTRIBUTION/AVAILABILITY STATEMENT
Distribution Statement A. Approved For Public Release; Distribution Unlimited

13. SUPPLEMENTARY NOTES

14. ABSTRACT

Many microelectromechanical systems (MEMS) use metal contact micro-switches as part of their reconfigurable device design. These devices utilize a mechanical component that can wear down and fail over time. Metal insulator transition (MIT) materials, also known as phase change materials (PCMs), exhibit a reversible transition that can be used to replace the mechanical component in reconfigurable devices. In the presence of a thermal or electric field stimuli, the PCMs will transition back and forth between a crystalline and amorphous state. During this transformation, the resistivity, reflectivity, and Young's modulus of the material drastically change. This research effort focuses on characterizing the stimuli required to transition germanium telluride (GeTe) and vanadium oxide (VOx). To do this, test structures were designed and micro-fabricated in AFIT's class 1000 cleanroom. The resistivity of the GeTe films underwent a volatile transition from 1.4E3Ohm-cm down to 2.28Ohm-cm and a nonvolatile transition from 1.4E3Ohm-cm to 2.43E-3Ohm-cm when a thermal stimulus was applied. The reflectivity of the film also changed significantly when crystallized, increasing over 30%. Lastly, the Young's modulus was measured and showed a 28% change during crystallization. After the materials were characterized, reconfigurable devices were designed to utilize the phase change properties of the PCMs.

15. SUBJECT TERMS
Microelectromechanical systems, phase change materials, germanium telluride, vanadium oxide, micro-switches

16. SECURITY CLASSIFICATION OF:			17. LIMITATION OF ABSTRACT	18. NUMBER OF PAGES	19a. NAME OF RESPONSIBLE PERSON
a. REPORT	b. ABSTRACT	c. THIS PAGE			Dr. Ronald A. Coutu, Jr.
U	U	U	UU	117	19b. TELEPHONE NUMBER *(Include area code)* (937) 255-3636 ext. 7230 (Ronald.Coutu@afit.edu)